### nature plants

Article

https://doi.org/10.1038/s41477-024-01788-8

## RNA helicase Brr2a promotes miRNA biogenesis by properly remodelling secondary structure of pri-miRNAs

Received: 31 January 2024

Accepted: 14 August 2024

Published online: 13 September 2024



Check for updates

Xindi Li <sup>1,6</sup>, Songxiao Zhong <sup>1,6</sup> ⋈, Changhao Li <sup>1</sup>, Xingxing Yan<sup>1</sup>, Jiaying Zhu <sup>1</sup>, Yanjun Li², Zhiye Wang <sup>3</sup>, Xu Peng <sup>4</sup> & Xiuren Zhang <sup>1,5</sup> □

RNA secondary structure (RSS) of primary microRNAs (pri-miRNAs) is a key determinant for miRNA production. Here we report that RNA helicase (RH) Brr2a, best known as a splice osome component, modulates the structural complexity of pri-miRNAs to fine tune miRNA yield. Brr2a interacts with microprocessor component HYL1 and its loss reduces the levels of miRNAs derived from both intron-containing and intron-lacking pri-miRNAs. Brr2a binds to pri-miRNAs in vivo and in vitro. Furthermore, Brr2a hydrolyses ATP and the activity can be significantly enhanced by pri-miRNAs. Consequently, Brr2a unwinds pri-miRNAs in vitro. Moreover, Brr2a variants with compromised ATPase or RH activity are incapable of unwinding pri-miRNA, and their transgenic plants fail to restore miRNA levels in brr2a-2. Importantly, most of tested pri-miRNAs display distinct RSS, rendering them unsuitable for efficient processing in brr2a mutants vs Col-0. Collectively, this study reveals that Brr2a plays a non-canonical role in miRNA production beyond splicing regulation.

RNA secondary structure (RSS) contains a new set of information that is interpreted and processed by specialized ribonucleoprotein complexes<sup>1</sup>. Through the complexes, RSS regulates diverse biological processes exemplified by miRNA production. MiRNAs are a group of small non-coding RNAs that guide Argonaute (AGO) proteins to repress expression of sequence-complementary target transcripts through degradation or translational repression<sup>2,3</sup>. MiRNAs are produced by the microprocessor that minimally comprises DCL1, HYL1 and SE proteins from pri-miRNAs in Arabidopsis<sup>2,3</sup>. Pri-miRNAs possess intrinsic hairpin structures providing codes to instruct the microprocessor of the precise cleavage at the correct positions. For instance, DCL1 measures a distance of 15-17 nucleotide (nt) away from a single-stranded (ss)double-stranded (ds) RNA junction region to start its first cleavage of pri-miRNAs<sup>4</sup>. DCL1 prefers to cut its substrate at the internal loops/ bulges or nearby sites in the stem regions<sup>4</sup>. Thus, the locations of the reference sites and stem-loop features of pri-miRNAs not only determine the orientation for launching the microprocessor, but also impact the accuracy and efficiency for miRNA production. However, plant pri-miRNAs are heterogeneous in their shapes and structures. Often, pri-miRNAs contain branched terminal loops that could trigger abortive processing of pri-miRNAs, leading to attenuation of productive processing<sup>4</sup>. In addition, RSS is dynamic and can be remodelled by an RNA helicase (RH). This scenario can be highlighted by the observation that Chromatin remodelling factors 2 (CHR2) can remodel RSS of pri-miRNAs, making them unsuitable substates and thus compromising miRNA production<sup>5</sup>.

Department of Biochemistry and Biophysics, Texas A&M University, College Station, TX, USA. 2State Key Laboratory for Managing Biotic and Chemical Threats to the Quality and Safety of Agro-products, Key Laboratory of Biotechnology in Plant Protection of MARA and Zhejiang Province, Institute of Plant Virology, Ningbo University, Ningbo, China. 3State Key Laboratory of Plant Physiology and Biochemistry, College of Life Sciences, Zhejiang University, Hangzhou, China. <sup>4</sup>Department of Medical Physiology, College of Medicine, Texas A&M University, College Station, TX, USA. <sup>5</sup>Department of Biology, Texas A&M University, College Station, TX, USA. <sup>6</sup>These authors contributed equally: Xindi Li, Songxiao Zhong. 🖂 e-mail: zhongsx@tamu.edu; xiuren.zhang@tamu.edu

Some species of pri-miRNA contain introns, and splicing out of introns from the pri-miRNAs is an essential step ahead of their processing by the microprocessor. Thus, defective splicing in the mutants of spliceosome components can impair pri-miRNA processing<sup>6,7</sup>. Some spliceosome members can enhance the transcription of *MIRNA* loci and promote the co-transcriptional assembly of the microprocessor, exemplified by Prp40 which typically functions as a U1 small nuclear ribonucleoprotein (snRNP) auxiliary protein<sup>8</sup>. Furthermore, spliceosome components, including Serrate-Associated Protein 1 (SEAP1, homologous to human SART3 and yeast Prp24)<sup>9</sup>, AAR2 (a U5 snRNP assembly factor)<sup>10</sup> and JANUS (homologue of the U2 snRNP assembly factor)<sup>11</sup>, can facilitate the formation of D-bodies where the microprocessor is often present. However, the mechanisms of spliceosome components appear to be diverse and their direct impact on pri-miRNA processing remains underexplored.

Brr2, a component of the spliceosome subunit U5, is well known for its canonical helicase function in unwinding the U4/U6 duplex to activate the spliceosome<sup>12</sup>. In contrast to other members of the Ski2-like family, Brr2 is characterized by its notably large molecular weight and two repeat RH cores (referred to as the N-helicase and C-helicase cassettes, respectively)13. In metazoans, upon binding to substrates, the Brr2 N-helicase hydrolyses ATP to facilitate its helicase function, thereby reshaping RNA substrates, whereas the C-helicase cassette lacks such a function but is able to stimulate the activity of the N-helicase cassette<sup>14</sup>. Furthermore, its conserved motif II (DEIH) and motif III (SAT) within the N-helicase cassette have been reported to be associated with ATPase and RH activities, respectively<sup>15,16</sup>. It has been also reported that superfamily 2 RHs can not only translocate along RNA to reshape its configuration, but also perform local strand unwinding in a non-processive manner<sup>1</sup>. Nevertheless, whether and how Brr2a has a novel function in any molecular processes other than splicing events is unknown.

Here we report that *Arabidopsis* Brr2a, the homologue of human Brr2, is a bona fide partner of the microprocessor, promoting levels of miRNAs derived from both intron-containing and intron-lacking pri-miRNAs. Brr2a was able to directly interact with pri-miRNAs in vivo and in vitro. The binding to pri-miRNA significantly enhanced the ATPase activity of Brr2a. Importantly, Brr2a exhibited the capability to unwind pri-miRNA substrates and the function relies on its DEIH and SAT motifs. Consequently, transgenic plants with these variants failed to restore miRNA levels in *brr2a-2*. Finally, dimethyl sulfate mutational profiling with sequencing (DMS-MaPseq) of the RSS of pri-miRNAs elucidated that Brr2a plays a pivotal role in ensuring the proper folding of most tested pri-miRNAs that is conducive to subsequent processing by the microprocessor. Thus, this study revealed that Brr2a, beyond its conventional involvement in splicing, plays a novel role in miRNA production.

#### Results

#### RH Brr2a is a new partner of the microprocessor

To identify new factors with the microprocessor, we mined the interactome of HYL1 (ref. 17) and SE<sup>18</sup>. Apart from DCL1 (ref. 19), CHR2 (ref. 5), HEN2 (ref. 18), RH6/8/12 (ref. 20) and RH11/37 (ref. 21), some other RHs with varying peptide reads were also recovered in the MS/MS analysis (Extended Data Fig. 1 and Supplementary Table 1). To explore whether the new candidates might have any potential correlation with the miRNA biogenesis pathway, we conducted an in silico transcriptome-wide association analysis with *DCL1* (ref. 22). Among the RHs, RH11 and RH37, which act in small RNA (sRNA) loading and/or stabilization in extracellular vesicles<sup>21</sup>, showed only moderate association of its expression dynamics with that of DCL1 (Extended Data Fig. 1, and Supplementary Tables 1 and 2). In contrast, *CHR2*, *Brr2a*, *Brr2c*, *CHR5* and *UPF1* displayed the most significant co-expression patterns with *DCL1* (Fig. 1a, Extended Data Fig. 1 and Supplementary Table 2). Among them, Brr2a (*AT1G20960*) was the only protein identified in

the proteomic datasets of both SE and HYL1. Whereas Brr2a has two homologues, Brr2b (*AT2G42270*) and Brr2c (*AT5G61140*), in *Arabidopsis*, only *Brr2a* showed ubiquitous expression (Extended Data Fig. 2a) and thus became our focus.

Next, we validated the association of Brr2a with microprocessor components. In co-immunoprecipitation (co-IP) assay, we could readily detect HYL1, but not SE or the control protein HSP70, in Brr2a co-immunoprecipitants (Fig. 1b). Importantly, the HYL1-Brr2a interaction is RNA independent as the addition of RNase did not decrease the amount of HYL1 in the immunoprecipitants of Brr2a (Fig. 1b). Notably, bimolecular fluorescence complementation (BiFC) assays showed that Brr2a could complement HYL1 when each was fused with an N- or C-terminal truncated portion of yellow fluorescent protein (YFP) (Fig. 1c), but this type of fluorescence complementation was not observed in the combinations of Brr2a with SE or DCL1 (Fig. 1c). Moreover, Brr2a showed co-localization with HYL1 when expressed in *Nicotiana benthamiana* (Extended Data Fig. 2b). These results indicate that Brr2a is a bona fide partner of HYL1 and might transiently interact with SE and DCL1.

The null mutation of Brr2a (brr2a-1) is embryo lethal. A hypomorphic allele of Brr2a mutant, cäö, hereafter referred as brr2a-2, harbours a point mutation within the N-helicase cassette (Extended Data Fig. 2c) and displays developmental abnormalities, including serrated leaves and early flowering<sup>23</sup>. Since *brr2a-2* is a weak allele, we generated transgenic plants using an artificial miRNA system<sup>24</sup> to knock down Brr2a transcripts (Extended Data Fig. 2d). The transgenic plants produced abundant amiR-Brr2a (Extended Data Fig. 2e), resulting in significant reduction of the Brr2a transcript in comparison with the wild-type control (Fig. 1d). Sequence alignment suggested that amiR-Brr2a might have certain sequence complementarity with two additional transcripts, AT2G18110 and AT1G27750, raising concerns of potential off-target effects (Extended Data Fig. 2f). However, these concerns were cleared by 5' rapid amplification of cDNA ends-polymerase chain reaction (RACE-PCR) and quantitative PCR with reverse transcription (RT-qPCR) assays, which detected neither the AGO-cleaved products from the two transcripts nor their expression changes in the transgenic plants vs Col-0 (Extended Data Fig. 2g,h). Thus, we named these amiR-Brr2a transgenic lines as brr2a-3. Notably, brr2a-3 phenocopied the morphological defects of brr2a-2, but with more severe phenotypes, including narrow and curly leaves, delayed plant growth, dwarfism and lesser rosette leaves before flowering (Fig. 1e.f). These developmental defects are reminiscent of hyl1-2 and se-2 (Fig. 1e,f), suggesting that Brr2a might have shared functions with the microprocessor components in regulating plant development.

#### Brr2a and HYL1 co-regulate genetic and miRNA pathways

Next, we performed RNA-seq analysis to examine the impact of Brr2a on the transcriptome. RNA-seq results further showed the significant reduction of Brr2a (Extended Data Fig. 3a). Moreover, we found 7,069 differentially expressed genes (DEGs) in brr2a-3 vs Col-0 (Fig. 1g and Supplementary Table 3). Among these DEGs, 3,155 and 3,914 genes were decreased and increased, respectively. Meanwhile, we observed that 1,170 and 2,627 DEGs were respectively downregulated and upregulated in hyl1-2 (ref. 25) (Fig. 1h,i). The number of DEGs in hyl1-2 was much smaller than that of brr2a-3, suggestive of a broader impact of loss-of-function mutation in brr2a-3 on the splicing process. Furthermore, there was a significant overlap of DEGs, with 958 upregulated and 413 downregulated genes shared between hyl1-2 and brr2a-3 (Fig. 1h,i). Conversely, when comparing the DEGs with opposite expression patterns, no significant overlap was found (Fig. 1h,i). Moreover, a similar pattern of DEGs was also observed between brr2a-3 and se-2 (ref. 26) (Extended Data Fig. 3b). Thus, RNA-seq analysis indicated that Brr2a and HYL1/SE might impact some genetic pathways in common in vivo.

Subsequent Kyoto Encyclopedia of Genes and Genomes (KEGG) analysis implicated the *brr2a-3*-upregulated genes in the spliceosome

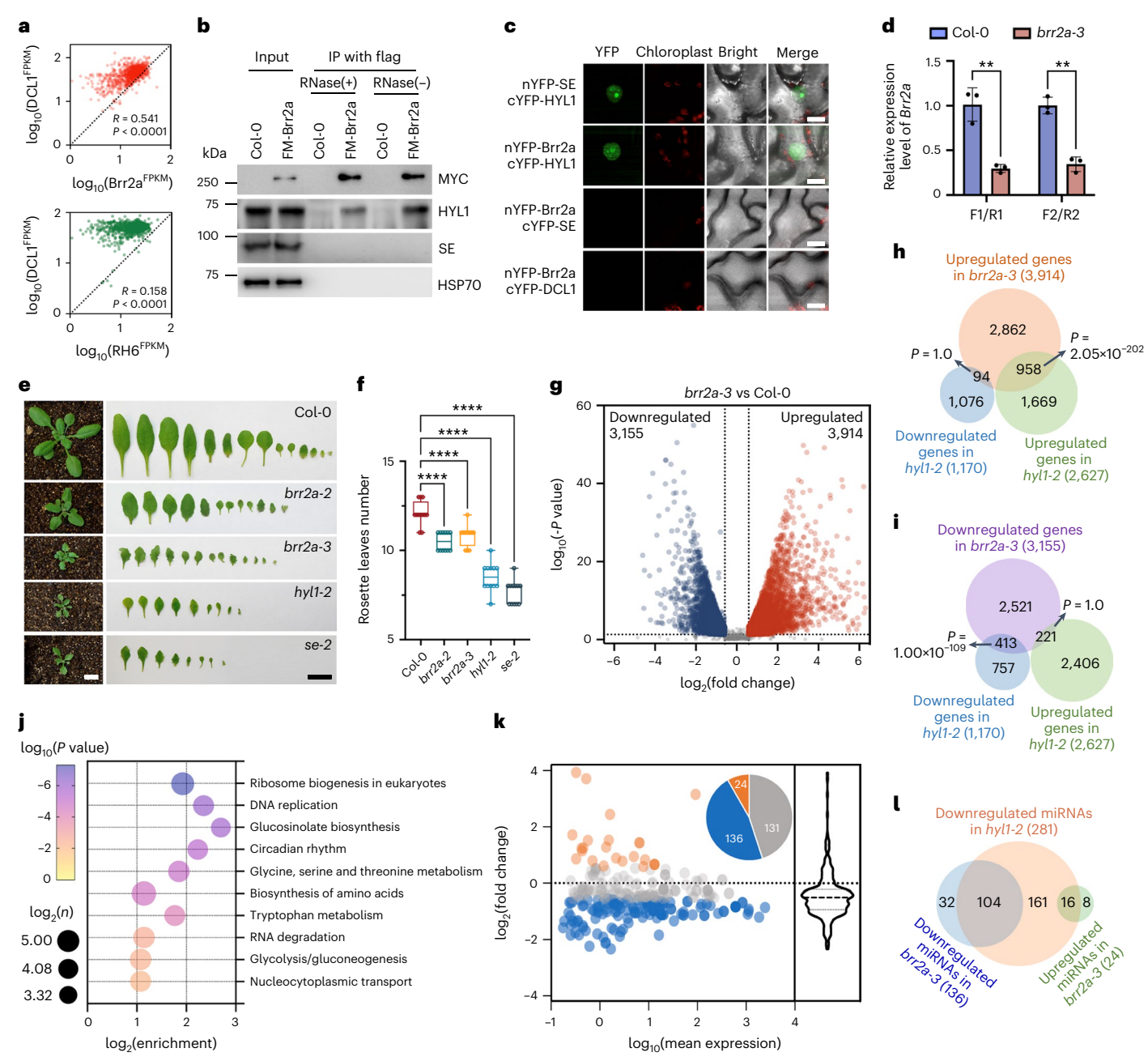


**Fig. 1**| RH Brr2a, a new partner of the microprocessor, contributes to RNA processing in *Arabidopsis*. a, Pan-transcriptome analysis shows synchronous transcriptome expression association between *DCL1* and *Brr2a*. *RH6* serves as a control. *R* values, Spearman's rank correlation coefficient. **b**, Co-IP assays confirm the interaction of Brr2a with HYL1 in *Arabidopsis*. Anti-Flag-M2 beads were used for IP in both the Col-0 and *brr2a-2*; *pBrr2a::FM-gBrr2a*. For RNase treatment, 10 μg ml<sup>-1</sup> of RNase A was added into plant lysates before IP. Immunoblots were detected by indicated antibodies. **c**, BiFC shows the interaction between Brr2a and HYL1, but not with DCL1 and SE, in *N. benthamiana*. Scale bars, 30 μm. **d**, RT–qPCR analyses show the reduced transcript level of *Brr2a* in *brr2a-3* vs Col-0 using two pairs of primers. F/R, forward/reverse primer. Data are mean ± s.d. of 3 biological replicates. **e**, Morphologic phenotype of *brr2a* mutants vs Col-0 and *hyl1-2*. At least 12 independent 3-week-old plants were photographed and representative images are shown. Scale bar, 1 cm. **f**, Statistical analysis of rosette leaves representing the

flowering time of mutants. Data are mean  $\pm$  s.e. of at least 12 independent plants. Lines, median; boxes, quartiles; whiskers, minimum to maximum.  $\bf g$ , A volcano plot exhibiting the DEGs in  $brr2a \cdot 3$  vs Col-0.  $\bf h$ ,  $\bf i$ , Overlapping of upregulated ( $\bf h$ ) and downregulated ( $\bf i$ ) genes in  $brr2a \cdot 3$  with DEGs in  $hyl1 \cdot 2$ . RNA-seq data for  $hyl1 \cdot 2$  were re-analysed with publicly available datasets  $^{25}$ .  $\bf j$ , KEGG enrichment of Brr2a and HYL1 co-regulated DEGs.  $\bf k$ , sRNA-seq analysis of miRNA profiling in  $brr2a \cdot 3$  vs Col-0. The lines in violin plots represent the median (dashed) and quartiles (dotted).  $\bf l$ , Venn diagram showing that the majority of miRNAs regulated by Brr2a belong to canonical HYL1-dependent subset  $^{27}$ . The blue, red and grey dots represent downregulated (Col-0/ $brr2a \cdot 3 \ge 1.5$ , P < 0.05), upregulated ( $brr2a \cdot 3$ /Col-0  $\ge 1.5$ , P < 0.05) and unchanged ( $\bf g$  and  $\bf k$ ) genes. At least three independent experiments were performed and representative images are shown ( $\bf b$  and  $\bf c$ ). Unpaired two-sided t-test ( $\bf a$ ,  $\bf d$  and  $\bf g$ ), one-way ANOVA with Dunnett's multiple comparisons test ( $\bf f$ ) and hypergeometric distribution test ( $\bf h$ ,  $\bf i$  and  $\bf j$ ); \*\*P < 0.01; \*\*\*\*P < 0.001 ( $\bf d$  and  $\bf f$ ).

pathway, probably due to feedback regulation of defective splicing in the mutant (Extended Data Fig. 3c). Other enriched pathways included ribosome biogenesis, glucosinolate biosynthesis, DNA replication, RNA degradation, and alanine, aspartate and glutamate

metabolism pathways (Extended Data Fig. 3c). On the other hand, the plant hormone signal transduction and circadian rhythm pathways exhibited downregulation in brr2a-3 vs Col-0 (Extended Data Fig. 3c). Notably, most of these pathways were also observed in DEGs shared by brr2a-3

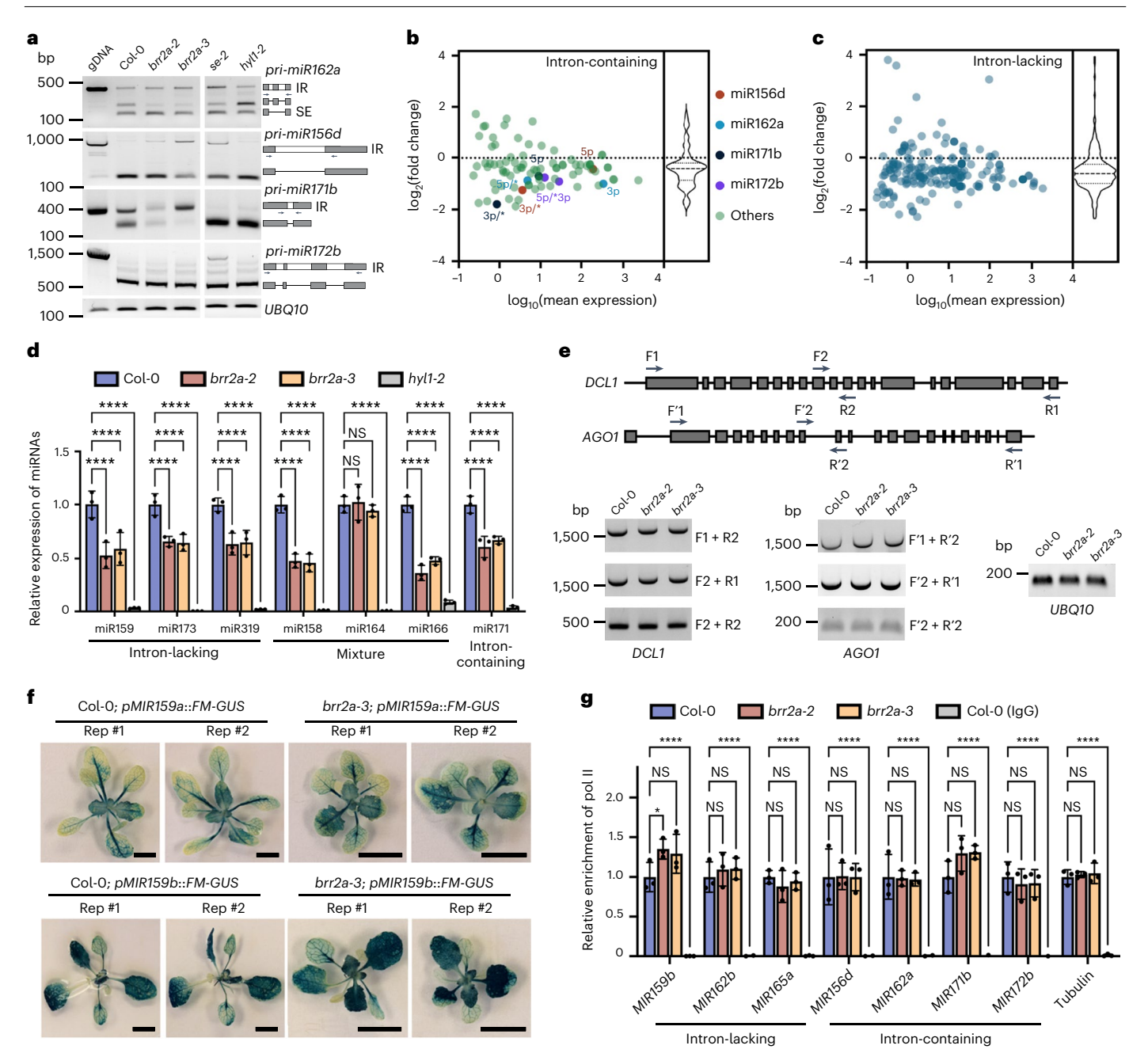


**Fig. 2** | **Brr2a** promotes the accumulation of miRNAs from both introncontaining and intron-lacking pri-miRNAs. a, RT-PCR results exhibit a defective splicing of pri-miRNAs in *brr2a* mutants vs Col-0. The gel pictures (left) and schematic illustration (right) display different PCR products and corresponding AS isoforms to scale. The grey and white boxes represent exons and introns, respectively. *UBQ10* served as a loading control. IR, intron retention; SE, skipped exon. **b,c**, Plots showing sRNA-seq profiles of miRNAs derived from intron-containing (**b**) and intron-lacking (**c**) pri-miRNAs. The *x* axis represents the expression of miRNAs in *brr2a-3*, the *y* axis the relative level of miRNAs in *brr2a-3* vs Col-0. The lines in violin plots represent the median (dashed) and quartiles (dotted). **d**, sRNA RT-qPCR validates the reduction of miRNA subsets in *brr2a* mutants vs Col-0. Each subset represents the miRNA originating from introncontaining, intron-lacking or mixed (both types of precursors) pri-miRNAs. *U6* was used as the internal loading control. **e**, Bottom: RT-PCR analysis reveals the

integrity of DCL1 and AGOI transcripts, the splicing of which was defective in some splicing-misfunctional mutants. Top: illustration of forward (F) and reverse (R) primers. Grey rectangles and lines represent exons and introns, respectively. UBQIO served as a loading control.  $\mathbf{f}$ , Histochemical staining of GUS performed with  $F_3$  segregation lines shows the comparable transcription of MIRI59a/MIRI59b in  $brr2a\cdot3$  vs Col-0. The mutant background plants were obtained by crossing Col-0 pMIRI59a/b::FM-GUS into  $brr2a\cdot3$ . Scale bars, 1 cm. See also Extended Data Fig. 5g for immunoblot analysis. Rep, replicate.  $\mathbf{g}$ , ChIP-qPCR shows that the enrichment of Pol II on MIRNA loci was not decreased in brr2a mutants vs Col-0. Tubulin served as an internal control. At least 3 biological replicates ( $\mathbf{a}$  and  $\mathbf{e}$ ) and 10 independent plants ( $\mathbf{f}$ ) were detected and representative images are shown. Data are mean  $\pm$  s.d. of 3 biological replicates ( $\mathbf{d}$  and  $\mathbf{g}$ ). Unpaired two-way ANOVA with Dunnett's multiple comparisons test ( $\mathbf{d}$  and  $\mathbf{g}$ );  $^{NS}P \ge 0.05$ ;  $^{*P} < 0.05$ ;  $^{****P} < 0.0001$  ( $\mathbf{d}$  and  $\mathbf{g}$ ).

and hyl1-2 (Fig. 1j), further suggestive of their possible co-regulatory impact on RNA processing.

We next assessed sRNA profiles in *brr2a-3* with Col-0 as a control (Extended Data Fig. 4a). The sRNA-seq analysis showed that the

portions of miRNA and trans-acting small interfering RNA (tasiRNA) were clearly reduced, whereas the sRNAs derived from ribosomal RNA (rRNA) increased in *brr2a-3* (Extended Data Fig. 4b). Further analysis showed that among 291 detectable miRNAs, 136 showed decreased

expression, whereas only 24 were upregulated in *brr2a-3* (Fig. 1k and Supplementary Table 4). Notably, most of the downregulated miR-NAs were HYL1 dependent<sup>27</sup> (Fig. 1l). Consistently, the expression of miRNA targets was broadly increased in *brr2a-3* vs Col-0 (Extended Data Fig. 4c). Taken together, these findings indicate that Brr2a has physical and genetic associations with the microprocessor, with further suggestion that the protein might function in the miRNA pathway.

#### Brr2a boosts miRNA yield via a splicing-independent route

Some pri-miRNAs contain introns, requiring coordinated processing with splicing and dicing events. It has been reported that alternative splicing (AS) of pri-miRNAs, as seen in se-2, can accumulate aberrant isoforms, thereby causing fluctuations in production of their cognate miRNAs<sup>28</sup>. We next detected whether Brr2a regulated AS of pri-miRNAs to modulate miRNA production. We found that pri-miR162a, which harbours two introns, exhibited increased isoforms of either skipped-exon or retention-intron. However, the functional isoform was reduced in brr2a mutants, reminiscent of se-2, compared with Col-0 and hyl1-2 (Fig. 2a). Consequently, miR162a levels were significantly reduced in brr2a mutants vs Col-0 (Fig. 2b). Similar splicing defects were also observed with pri-miR156d and pri-miR171b among others. These splicing defects probably reduced the amount of processable forms of pri-miRNAs and at least partially contributed to decreased accumulation of miRNAs in the mutants vs Col-0 (Fig. 2a,b). These results suggest that Brr2a could indeed exert a canonical role in splicing to promote miRNA production.

Notably, although pri-miR172b exhibited proper splicing in *brr2a* mutants, as observed in Col-0 and *hyl1-2*, it still produced less mature miR172b (Fig. 2a,b). Thus, we hypothesized that Brr2a might act in a splicing-independent mechanism to facilitate miRNA production. To test this, we revisited the sRNA-seq data, categorizing miRNAs into two groups on the basis of their origin—either intron-containing or intron-lacking pri-miRNAs. Surprisingly, we observed a notable reduction in mature miRNAs that were derived not only from intron-containing pri-miRNAs (33/87) (Fig. 2b) but also from those lacking introns (103/204) (Fig. 2c). Moreover, more cases were readily validated by RT–qPCR (Fig. 2d), suggestive of a potential novel function of Brr2a beyond its canonical role in splicing.

Splicing defects on the transcripts of microprocessor components could lead to a decrease in miRNA production<sup>29</sup>. To test this possibility, we assessed the transcript integrity of microprocessor and RNA-induced silencing complex components in *brr2a* mutants. First, both RNA multivariate analysis of transcript splicing (rMATS) and Integrative Genomics Viewer (IGV) files indicated that the splicing patterns of *SE,DCL1* and *HYL1* among other transcripts showed no obvious defect in *brr2a-3* vs Col-0 (Extended Data Fig. 5a,b and Supplementary Table 5). Next, RT–PCR analysis further confirmed that the splicing machinery in *brr2a* mutants could still ensure the completion of *DCL1* and *AGO1* transcripts, probably due to the hypomorphic nature of *brr2a* alleles and/or the functional redundancy of Brr2b and 2c (Fig. 2e). Neither the transcript nor protein levels of *AGO1*, *DCL1* and *SE* were reduced

in *brr2a-3* compared with those of Col-0 (Extended Data Fig. 5c,d). Intriguingly, we observed a significant upregulation of both RNA and protein levels of HYL1 in the *brr2a* mutants (Extended Data Fig. 5c,d). These accumulations probably resulted from feedback regulation, which parallels the previously noted upregulation of the spliceosome pathway in *brr2a-3* (Extended Data Fig. 3c). Despite this, the formation of dicing bodies was seemingly unaffected in *brr2a-3* vs Col-0 (Extended Data Fig. 5e). In addition, the expressions of other key components in the miRNA pathway were not reduced (Extended Data Fig. 5f). Hence, these data further suggest a splicing-independent function of Brr2a in miRNA production.

#### Brr2a does not affect the transcription of MIRNA loci

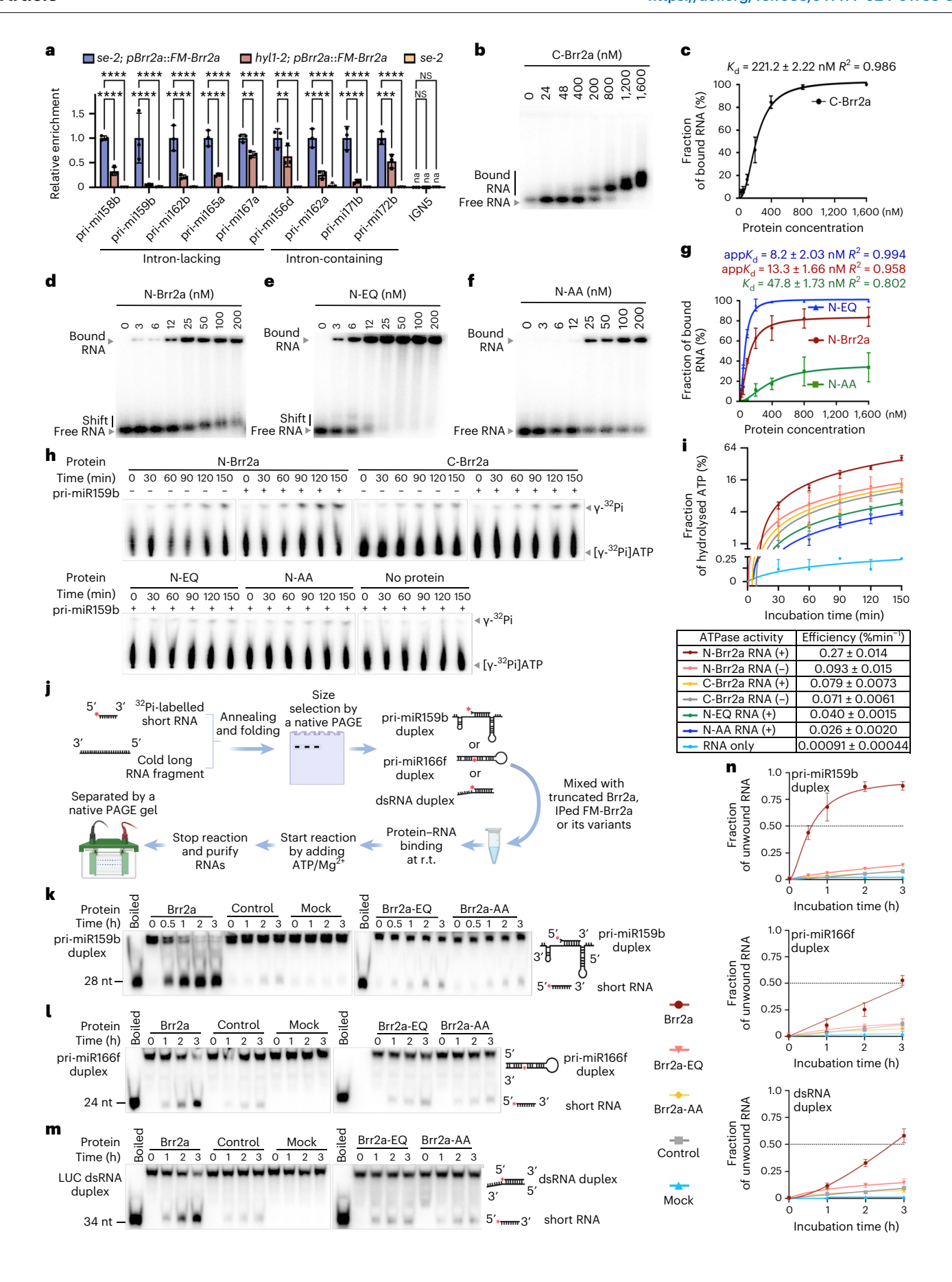
We then investigated whether Brr2a was involved in the transcriptional machinery at MIRNA loci. Our initial focus was on MIR159a and MIR159b, which generate pri-miR159a and pri-miR159b, respectively, with both lacking introns and producing less mature miRNAs in brr2a-3 (Supplementary Table 4). We crossed the pMIR159a/b::Flag-4xMYC (FM) -β-glucuronidase (GUS) transgenic lines with brr2a-3 separately and analysed the GUS reporter transcription in the brr2a-3 homozygote background from F<sub>3</sub> segregation lines. Through GUS staining assays and western blot analysis, we found comparable and slightly increased accumulation levels of GUS for MIR159a and MIR159b in brr2a-3 vs Col-0, respectively (Fig. 2f and Extended Data Fig. 5g). This prompted us to further investigate the transcription level of MIR159b in brr2a mutants via a Pol II chromatin immunoprecipitation (ChIP) assay. Again, the overall Pol II occupancy on MIR159b slightly increased in brr2a mutants vs Col-0 (Fig. 2g). For other tested loci, Brr2a did not alter their transcription, regardless of whether pri-miRNAs have introns or not (Fig. 2g). Taken together, we conclude that Brr2a does not influence miRNA production via promoting MIR transcription.

#### Brr2a directly binds to pri-miRNAs

We next hypothesized that RH Brr2a might bind to pri-miRNAs and modulate their RSS, thereby affecting miRNA production. Since Brr2a's canonical unwinding activity relies on the U4/U6 duplex structure14,30,31, we first examined whether pri-miRNA could serve as a substrate for Brr2a. To test this, we generated transgenic plants carrying pBrr2a::FM-gBrr2a in the se-2 and hyl1-2 backgrounds, where pri-miRNAs were substantially accumulated due to defective processing. We then performed ribonucleoprotein immunoprecipitation (RIP) assays using anti-Flag antibodies, with se-2 as a control. The RIP-qPCR results revealed a significant enrichment of pri-miRNAs in Brr2a's immunoprecipitates compared with the control IP, regardless of whether they contain introns (for example, pri-miR156d, pri-miR162a, and pri-miR171b and 172b) or lack introns (for example, pri-miR159b, pri-miR162b and so on) (Fig. 3a). Conversely, IGN5, a non-coding RNA transcribed by Pol V<sup>32</sup>, was only detectable in the input but not in the immunoprecipitates (Fig. 3a). Notably, the association of Brr2a with pri-miRNAs was also detectable in the hyl1-2 background, but the amount was significantly reduced in hyl1-2 vs se-2 (Fig. 3a). Taken together, we conclude

**Fig. 3** | **RH Brr2a binds and remodels pri-miRNAs. a**, RIP assays show that Brr2a could bind intron-containing and intron-lacking pri-miRNAs in vivo. IPs were conducted with anti-Flag M2 beads, and the resulting Brr2a-bound RNAs were then used for RT-qPCR analysis. The se-2 and Pol V transcript IGN5 served as negative control plant and RNA, respectively. Unpaired two-way ANOVA with Dunnett's multiple comparisons test;  $^{NS}P \ge 0.05$ ;  $^{**P} < 0.001$ ;  $^{***P} < 0.0001$ .  $^{**P} < 0.0001$ .  $^{***P} < 0.0001$ .  $^{**P} < 0.0001$ .  $^{***P} < 0.0001$ .  $^{***P} < 0.0001$ .  $^{**P} < 0.0001$ .  $^{*$ 

three kinds of dsRNA duplexes and performing unwinding assay. See Methods for details. r.t., room temperature.  $\mathbf{k}-\mathbf{m}$ , Results of RNA native PAGE gels reveal the accumulation of released ssRNA from pri-miR159b duplex ( $\mathbf{k}$ ), pri-miR166f duplex ( $\mathbf{l}$ ) and dsRNA duplex with a 3′ overhang ( $\mathbf{m}$ ) in unwinding assays.  $\mathbf{n}$ , Statistical analysis of unwinding assays. Both paired and unpaired RNAs were quantified to generate the curves fitting the Michaelis–Menten model, with s.d. from 3 independent experiments.  $\mathbf{b}-\mathbf{i}$ , N/C-Brr2a represents N/C-terminal truncated Brr2a; N-EQ or N-AA represents the variants of N-Brr2a carrying mutations E640Q or S676A and T678A.  $\mathbf{j}-\mathbf{n}$ , Brr2a-EQ and Brr2a-AA represent the variants of full-length Brr2a carrying mutations E640Q and S676A T678A, respectively. Data are mean  $\pm$  s.d. of 3 biological replicates ( $\mathbf{a}$ ,  $\mathbf{c}$ ,  $\mathbf{g}$ ,  $\mathbf{i}$  and  $\mathbf{n}$ ). At least 3 independent experiments were performed and representative images are shown ( $\mathbf{b}$ ,  $\mathbf{d}-\mathbf{f}$ ,  $\mathbf{h}$  and  $\mathbf{k}-\mathbf{m}$ ).



that Brr2a directly binds to both intron-containing and intron-lacking pri-miRNAs in vivo and the association is facilitated by HYL1. This observation is further supported by a recent RNA pull-down analysis using intron-lacking pri-miR398 as the bait that recovered Brr2a as one of pri-miRNA binding proteins<sup>33</sup>.

We next studied whether Brr2a bound to pri-miRNAs in vitro. Since purification of the full-length Brr2a was undoable from E. coli, we generated N- (487–1,288 aa, N-Brr2a) or C- (1,289–2,171 aa, C-Brr2a) helicase cassettes of Brr2a variants, each encompassing a full-length helicase cassette (Extended Data Figs. 2c and 6a). Electrophoretic mobility shift assays (EMSAs) showed that C-Brr2a exhibited a weak binding affinity to folded pri-miR159b, with a  $K_{\rm d}$  of -221.2  $\pm$  2.2 nM (Fig. 3b,c and Extended Data Fig. 6b). In sharp contrast, N-Brr2a displayed a robust binding affinity to folded pri-miR159b, with a  $K_{\rm d}$  of -13.3  $\pm$  1.7 nM (Fig. 3d,g and Extended Data Fig. 6b).

To further study whether the association of N-Brr2a with primiRNAs depended on its ATPase or helicase activity, we generated N-Brr2a variants with compromised ATPase activity (N-EQ, E640Q) or defective helicase function (N-AA, N-S676A T678A), targeting two motifs that are highly conserved in animals, plants and fungi (Extended Data Figs. 2c and 6a). EMSA assays uncovered distinct effects of the two mutations on RNA binding affinity. The N-EQ seemingly increased RNA retention within the RNP, with a 1.5-fold enhancement in binding affinity with an app $K_d$  (apparent  $K_d$ ) of ~8.2 ± 2.0 nM (Fig. 3e,g and Extended Data Fig. 6b). Conversely, the N-AA mutation hindered the formation of the RNP complex, resulting in a 3.5-fold reduction in RNA binding affinity compared with that of N-Brr2a with a  $K_d$  of ~47.8 ± 1.7 nM (Fig. 3f,g and Extended Data Fig. 6b). However, when switching to ssRNA, all proteins exhibited negligible RNA binding affinity (Extended Data Fig. 6c-e). Taken together, we conclude that Brr2a, mainly relying on its N-terminal helicase domain, could bind to pri-miRNAs.

#### ATPase/RH activity of Brr2a can be stimulated by pri-miRNAs

We then investigated whether Brr2a exhibited ATPase activity. In vitro ATPase reconstitution followed by thin layer chromatography (TLC) assays showed that both N-Brr2a and C-Brr2a exhibited weak capability to hydrolyse ATP in the absence of RNA. Specifically, N-Brr2a hydrolysed ~0.093% 32[P]ATP supplied per min, showing slightly stronger activity than C-Brr2a, which hydrolysed ~0.07% ATP per min (Fig. 3h,i, Extended Data Fig. 7a and Supplementary Table 6). Notably, the ATP hydrolysis activity of N-Brr2a, but not C-Brr2a, was significantly stimulated upon the supply of pri-miR159b, resulting in ~3-fold increase, hydrolysing ~0.27% ATP per min (Fig. 3h,i, Extended Data Fig. 7a and Supplementary Table 6). Notably, both ATPase activity and the stimulation were eliminated by EQ and AA mutations, as the two variants barely hydrolysed the ATP (Fig. 3h,i, Extended Data Fig. 7a and Supplementary Table 6). These observations are reminiscent of previous findings that motif II (DEIH) accounts for ATPase activity  $^{15,16}$  and motif III (SAT motif) is required for both helicase activity and ATPase activity<sup>34–36</sup>. Thus, these results suggest that pri-miR159b could stimulate the ATPase activity of Brr2a.

We hypothesized that Brr2a might unwind pri-miRNAs in vitro. To test this, we first detected whether truncated Brr2a and its variants could unwind a dsRNA duplex of pri-miR159b. This dsRNA duplex was generated by annealing the 3′ flanking single-stranded region of pri-miR159b with a short <sup>32</sup>P-labelled RNA fragment, resulting in a complicated structure with a 3′ stem loop, central ssRNA and stem region, and a 5′ stem loop, reminiscent of core domain and stem loops of U4 in the U4/U6 duplex <sup>37</sup> (Fig. 3j). Unwinding assays found that the N-terminal cassette, but not the C-terminal cassette, of Brr2a could release certain portions of the ssRNA from the dsRNA duplex (Extended Data Fig. 7b). Furthermore, the helicase activity of N-Brr2a depended on its DEIH and SAT motifs (Extended Data Fig. 7b). We next investigated the helicase activity of full-length Brr2a and its variants with compromised activities of ATPase or helicase immunoprecipitated from transgenic plants (Extended Data Fig. 7c). For this assay, we generated

two other types of dsRNA duplexes: a nicked pri-miR166f duplex that contained a stem-loop RNA structure<sup>5</sup> and a full-paired dsRNA duplex with a ~110 nt 3′ overhang<sup>38</sup> (Fig. 3j). Interestingly, wild-type Brr2a readily displaced a majority of the short RNA fragments from the pri-miR159b duplex, whereas two variants (Brr2a-EQ and Brr2a-AA) did not, as the amount of released free short RNA from these variants was comparable to that from the control IP (Fig. 3k and Extended Data Fig. 7d). Furthermore, Brr2a could still unwind the nicked pri-miR166f and dsRNA duplex and exhibited comparable efficiencies for these substrates (Fig. 3l,m and Extended Data Fig. 7d), although it was less efficient than with the pri-miR159b duplex (Fig. 3n). Together, these results indicate that plant Brr2a could promiscuously remodel substrates with different structures.

#### Helicase activity of Brr2a is required for miRNA production

To further investigate whether helicase activity is necessary for Brr2a to promote miRNA production, we generated transgenic complementation plants in the brr2a-2 background expressing either ATPase activity-compromised variant Brr2a-EQ (brr2a-2 pBrr2a::FM-Brr2a-EQ, E640Q) or RH function compromised variant Brr2a-AA (brr2a-2 pBrr2a::FM-Brr2a-AA, S676A T678A) driven by the Brr2a native promoter. While pBrr2a::FM-Brr2a transgenic plant could fully rescue the morphologic defect of brr2a-2 (Fig. 4a,b), the transgenic plants carrying the two variants still exhibited developmental defects as seen in brr2a-2 (Fig. 4a,b). Consistently, these plants showed significant reduction in the levels of miRNAs derived from both intron-containing and intron-lacking pri-miRNAs in the transgenic plants (Fig. 4c). The mutations in ATPase and helicase activities did not impact the Brr2a interaction with HYL1 (Fig. 4d). However, the RIP assays showed that the EQ variant was enriched with even more pri-miRNAs compared with Brr2a. Clearly, the Brr2a-EQ-bound pri-miRNAs did not proceed for processing in the hypomorphic alleles (Fig. 4e and Extended Data Fig. 7e). By contrast, Brr2a-AA variant formed less stable or impaired pri-miRNA-protein complexes (Fig. 4e and Extended Data Fig. 7e). These results are consistent with their differential RNA-binding affinities in EMSA (Fig. 3b-g). Taken together, these results indicate that the proper helicase activity of Brr2a is indeed essential for miRNA production in plants.

#### Brr2a modulates overall RSS patterns of pri-miRNAs

We next assessed how Brr2a impacted RSS of pri-miRNAs in vivo by conducting DMS-MaPseq. Briefly, in DMS-MaPseq, DMS treatment of living Arabidopsis plants induces modifications specifically on unpaired adenosine (A) and cytosine (C) residues. These modified bases introduce mutations during the reverse transcription process that can be decoded via high-throughput sequencing analysis, enabling us to profile mutational rates to capture RSS of pri-miRNAs in vivo<sup>3</sup> (Extended Data Fig. 8a). In DMS-MaPseq analysis, we found a significant increase in mismatch ratios at A and C positions compared with G and U in all samples, confirming the success of the DMS treatment (Extended Data Fig. 8b). We next calculated Gini indexes of pri-miRNAs to reflect the variation of RSS in the transcripts. Typically, a higher Gini index indicates more structured and paired regions in RNAs. Interestingly, the Gini index was significantly increased in brr2a-3 compared with Col-0, indicating that pri-miRNAs were indeed more structured in the mutant vs Col-0 (Fig. 5a).

Because of the heterogenicity in shapes and lengths, plant pri-miRNAs can be processed from the base to loop (BTL), from loop to base (LTB) or even bidirectionally  $^{4,40}$ . In this scenario, we divided the pri-miRNAs with reduced miRNA production in  $\it brr2a-3$  into two categories of BTL and LTB, and then performed ensembled DMS-MaPseq analysis separately. For the BTL-processed pri-miRNAs, DMS displayed higher but varying activities at the sites of -17 to -13 nt and -9 to -5 nt in the 5' end lower stem regions of pri-miRNAs in Col-0, indicative of internal loops or bulges in the regions (Fig. 5b). Importantly, DMS activity

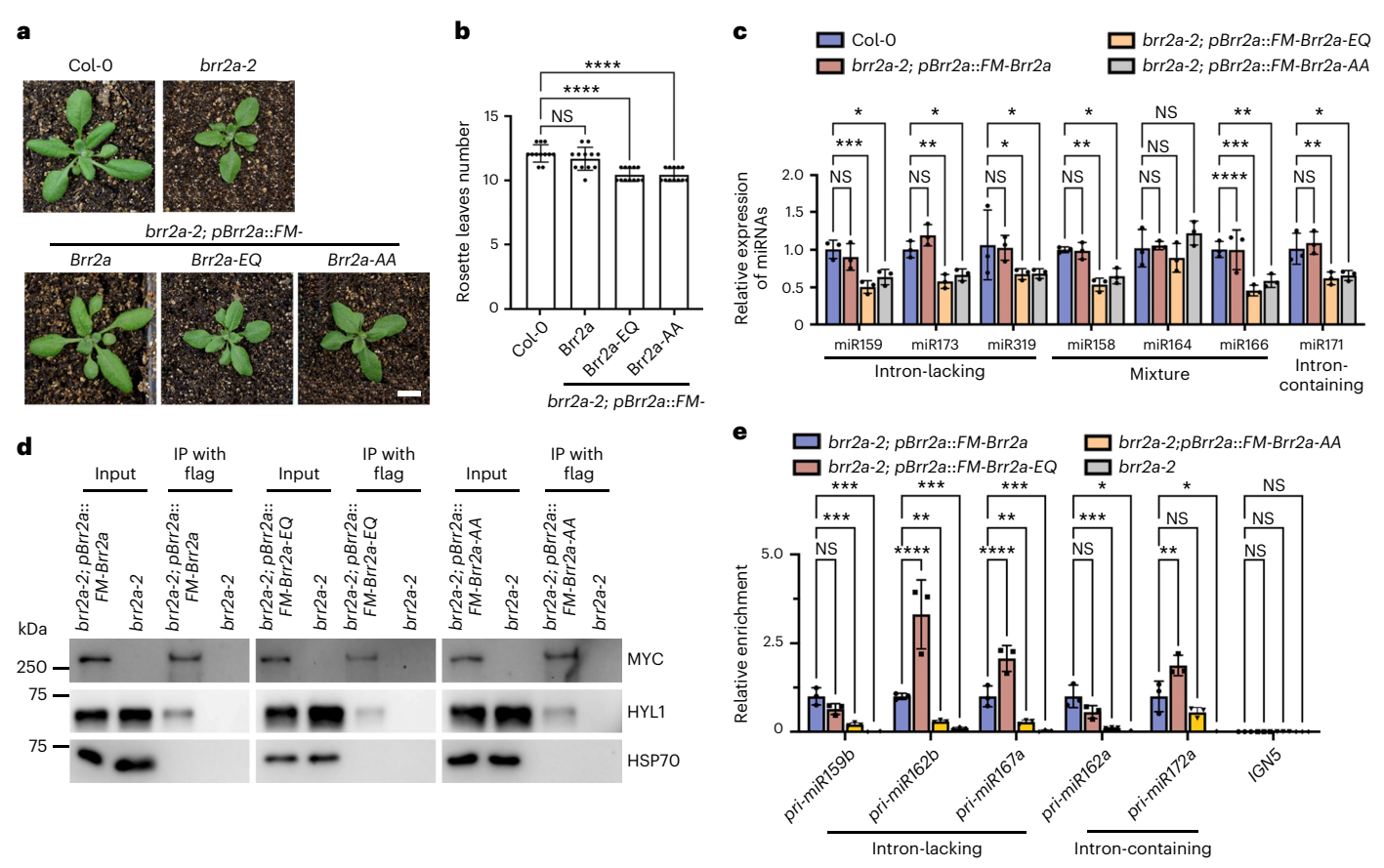


**Fig. 4** | **Helicase activity of Brr2a is essential for plant development and miRNA production. a,b**, Morphologic pictures of 3-week-old plants (**a**) and statistical analysis of rosette leaves number (**b**) show defective development of *brr2a-2* complemented with mutated *Brr2a*, with *brr2a-2 pBrr2a::FM-Brr2a* serving as a positive control. Data are mean ± s.e. of at least 12 independent plants. Scale bar, 1 cm. **c**, sRNA RT–qPCR validates the reduction of tested miRNAs in the complementation lines expressing wild-type Brr2a and its variants vs Col-0. The miRNA subsets that originate from intron-containing, intronlacking or both types of precursors are shown. *U6* was used as internal loading control. **d**, Co-IP assays validate the interaction of HYL1 and Brr2a variants in complementation lines. Anti-flag M2 beads were used for IP, and proteins were detected by antibodies against MYC, HYL1 and HSP70. **e**, RIP RT–qPCR assays

show that Brr2a variants bound different amounts of pri-miRNAs in vivo. IPs were conducted with anti-flag M2 beads. Pol V transcript IGN5 served as negative control RNA. Quantification was performed by normalizing the amount of Brr2a variant IP-derived RNA to that of the immunoprecipitated proteins and then to that of wild-type Brr2a where the ratio was arbitrarily set as 1. See also Extended Data Fig. 7e for western blot analysis of IP samples.  $\mathbf{a}$ - $\mathbf{e}$ , Brr2a-EQ and Brr2a-AA represent the variants of full-length Brr2a carrying mutations E640Q and S676A T678A, respectively. At least 12 independent plants ( $\mathbf{a}$  and  $\mathbf{b}$ ) and 3 biological replicates ( $\mathbf{d}$ ) were detected, and representative images are shown. Data are mean  $\pm$  s.d. of 3 biological replicates ( $\mathbf{c}$  and  $\mathbf{e}$ ). One-way ( $\mathbf{b}$ ) and two-way ( $\mathbf{c}$  and  $\mathbf{e}$ ) ANOVA with Dunnett's multiple comparisons test;  $^{NS}P \ge 0.05$ ;  $^*P < 0.05$ ;  $^*P < 0.05$ ;  $^*P < 0.01$ ;  $^*P < 0.001$ ;  $^*P < 0.001$ ;  $^*P < 0.001$  ( $^*P < 0.001$ ),  $^*P < 0.001$  ( $^*P < 0.001$ ), and  $^*P < 0.001$ ;  $^*$ 

profiling along the lower stem regions showed altered patterns in the brr2a-3 vs Col-0 (Fig. 5b). For instance, we observed decreased DMS activities at -17 to -15 nt in the 5' lower arms in brr2a-3, but increased and varying DMS activities at -14 nt to -13 nt, indicating a shifting of internal reference loops from -17 to -15 nt to -14 to -13 nt in the 5' lower arms of pri-miRNAs in brr2a-3 vs Col-0 (Fig. 5b, green dashed box). In parallel, we detected decreased DMS activities at 15 nt and 12 nt in 3' arms lower stems in *brr2a-3*, and increased DMS activities at 14 nt and 13 nt, which suggested a marginal shift of the reference loops from 15-14 nt to 13-12 nt at the 3' arms of lower stems at these pri-miRNAs in brr2a-3 vs Col-0 (Fig. 5c, green dashed box). Furthermore, increased sizes of the internal loops at the -9 to -6 nt (Fig. 5b, red dashed box) positions at the 5' arm and 4–6 nt (Fig. 5b, pink dashed box) and 13-14 nt (Fig. 5b, blue dashed box) positions in the miRNA/\* duplexes, as well as coordinated increase of 6–3 nt (Fig. 5c, red dashed box) positions at the 3' arm and -5 to -7 nt (Fig. 5c, pink dashed box) and -13 to -14 nt (Fig. 5c, blue dashed box) positions in the miRNA/\* duplexes, were seemingly observable in the pri-miRNAs in the brr2a-3 vs Col-0. All these changes could be expected to have adverse impacts on pri-miRNA processing.

Computational analysis of the LTB-processed pri-miRNAs became more complicated than the BTL-patterned ones as many of the LTB pri-miRNAs were sequentially processed before reaching the miRNA/\* duplexes $^4$ l. However, we could observe variations in DMS activity in the upper stems and terminal loops between brr2a-3 and Col-0 (Extended Data Fig. 8c). Such difference might be meaningful as the internal loops in this region significantly impacted the production of mature miRNAs. In addition, the high and contrasted variations in DMS activities in the duplex regions of both brr2a-3 and Col-0 were also detectable.

#### Brr2a contributes to RSS of pri-miRNA for processing

Due to heterozygosity of pri-miRNAs in plants, ensembled DMS-MaPseq did not allow us to simply conduct statistical significance tests of DMS reactivity in each position because individual pri-miRNAs have their internal loops/bulges that are of viable sizes and in different sites. Alternatively, Brr2a might not act on the same locations of all pri-miRNAs. To accurately decipher the precise impact of Brr2a on RSS remodelling for all pri-miRNAs, we focused on a handful pri-miRNAs that were of sufficient reads, and thoroughly assessed the structural changes of the pri-miRNAs in *brr2a-3* vs Col-0. Pri-miR158a follows a BTL-typed

processing. In this scenario, the microprocessor sets the first cleavage site at 15-17 nt away from its ssRNA-dsRNA internal reference site at the basal region (Fig. 5d). Whereas DCL1 prefers to cut pri-miRNAs at the edge of small internal loops or mismatches in wild-type plants, an enlarged internal loop at the first cleavage site would suppress miR158 production in the brr2a-3 vs Col-0. Similar patterns were also observed with pri-miR170 and pri-miR172b. For these pri-miRNAs, the initial reference ssRNA-dsRNA junction regions at the lower stems became obscure in brr2a-3 vs Col-0 (Extended Data Fig. 9a). Furthermore, the numbers and sizes of internal loops/bulges were increased in both the lower stems and the miRNA/\* duplex regions of pri-miRNAs in the brr2a-3 vs Col-0. Two pri-miRNAs, pri-miR172a and pri-miR844a, also followed this change. Moreover, these two pri-miRNAs also exhibited increased DMS activities in the upper stems, indicative of unpaired structures in brr2a-3 vs Col-0 (Fig. 5e and Extended Data Fig. 9b). This change would increase the likelihood of pri-miRNA processing from LTB, consequently impairing productive processing.

Pri-miR159a is processed from an LTB direction, and four sequential cleavages are entailed to successfully release mature miR159a/\* duplex. This pri-miRNA produced a remarkable high reads number of mature miR159 but significantly reduced reads of intermediate products (~60,000 vs 300) in Col-0, whereas the opposite pattern (35,000 vs 2,000) was observed in *brr2a-3* (Fig. 5f). This contrast was pronounced and clearly resulted from the structural difference of pri-miR159a in Col-0 vs brr2a-3. The microprocessor favours the cutting sites at or close to the internal loops. Here, pri-miR159a had several hotspots of DMS reactivity, indicative of internal loops or mismatches, along the upper stems in both Col-0 and brr2a-3 (Fig. 5g). However, these internal loops or mismatches were intriguingly located at or adjacent to the cutting sites in Col-0, potentially facilitating processivity of DCL1 activity from the terminal loop to the lower base. By contrast, the cleavage sites were in relatively more folded regions of the upper stem in brr2a-3 which would be considered as a suboptimal structure for DCL1 function, hindering its processivity. Furthermore, DMS activity hotspots were also detected in the middle of the first set of sRNA/\* duplexes (with 1,267 and 404 reads) in brr2a-3 that did not promote DCL1 to proceed with the processing. In addition, the lower stem of pri-miR159a harboured a bigger basal loop in Col-0, whereas the nucleotides in the counterpart regions were much more paired in *brr2a-3* (Fig. 5g). This conformation is likely to further inhibit accurate and efficient processing of miRNA/\* from pre-miRNAs in the mutant vs Col-0, as both animal Dicer and plant DCL1 recognize the loop-bulge structures in addition to the 5' and 3' ends of pre-miRNAs for accurate processing4,42.

Similar to pri-miR159a, pri-miR162a and pri-miR400 are processed from LTB. The pri-miRNAs exhibited a smaller terminal loop that were less instructive to DCL1 (Extended Data Fig. 9c). Notably, there were larger loops in the lower stems but located -10 nt away from the miRNA/\* duplexes of pri-miR162a and pri-miR400 in *brr2a-3*, but how

this change affects miRNA production is uninterpretable based on our current understanding of the microprocessor mechanism.

Pri-miRNAs with branched terminal loops or big terminal loops are subjected to bidirectional processing, leading to a dynamic of productive and abortive processes<sup>5</sup>. Pri-miR165a has previously been predicted to have a structure of branched terminal loops according to RNAfold that is solely grounded on a thermostability algorithm<sup>4</sup>. However, it has been a mystery that this pri-miRNA produces substantial amount of miR165a even with a predicted branched terminal loop. In fact, DMS activity was detectable but weak in the upper stem in Col-0, suggesting that pri-miR165a is in a dynamic transition between the linear folded hairpin and a structure with a terminal branched loop in vivo, underscoring its capacity to produce abundant miR165 as observed in pri-miR165b<sup>4</sup> (Fig. 5h). Surprisingly, pri-miR165a exhibited much stronger DMS activity indicative of a structure with standardized branched terminal loops in *brr2a-3*, which would trigger abortive processing and resultant lower accumulation of miR165 in the mutant.

Different from other miRNAs, miR157a and miR2112, whose pri-miRNAs are processed from LTB, were accumulated in *brr2a-3* vs Col-0. Interestingly, both pri-miR157a and pri-miR2112 have more unpaired regions in the upper stem in *brr2a-3* vs Col-0, indicating a greater propensity to produce higher levels of miR157a and miR2112, respectively (Extended Data Fig. 9d). Our DMS-MaPseq analysis also detected increased DMS activities in pri-miR164a, suggestive of more mismatches in the mutant vs Col-0 (Extended Data Fig. 9e). Interestingly, these positions with increased DMS activities were mainly located within pre-existing internal and terminal loops, which did not obviously alter the RSS of pri-miR164a and miR164 production (Fig. 2d and Supplementary Table 4). Taken together, these results suggest that Brr2a is typically involved in remodelling the secondary structure of pri-miRNAs for their proper processing, whereas in a very few cases, the protein might hinder the production of miRNAs (Fig. 6).

#### **Discussion**

Here we report a non-canonical function of Brr2a and elucidate its new mechanism in miRNA biogenesis. While Brr2a could act as an essential spliceosome component to regulate the splicing of intron-containing pri-miRNAs to generate processable forms of pri-miRNAs for the microprocessor, this very protein could also be recruited by HYL1 and directly associate with pri-miRNAs, utilizing its helicase activity to modulate their RSS to present generally more optimally structured substrates for DCL1, resulting in increased accumulation of miRNAs.

Mechanistically, Brr2a represents a distinctive paradigm wherein helicase activity is employed to restructure pri-miRNAs, thereby facilitating their processing and increasing miRNA yield. This is different from our earlier-reported RH CHR2 which typically remodels pri-miRNAs to inhibit their processing, leading to reduced miRNA production<sup>5</sup>. Several other RHs, such as RH6/8/12 (ref. 20), MAC7 (ref. 17) and Prp28 (SMA1)<sup>29</sup>, have been reported to contribute to miRNA

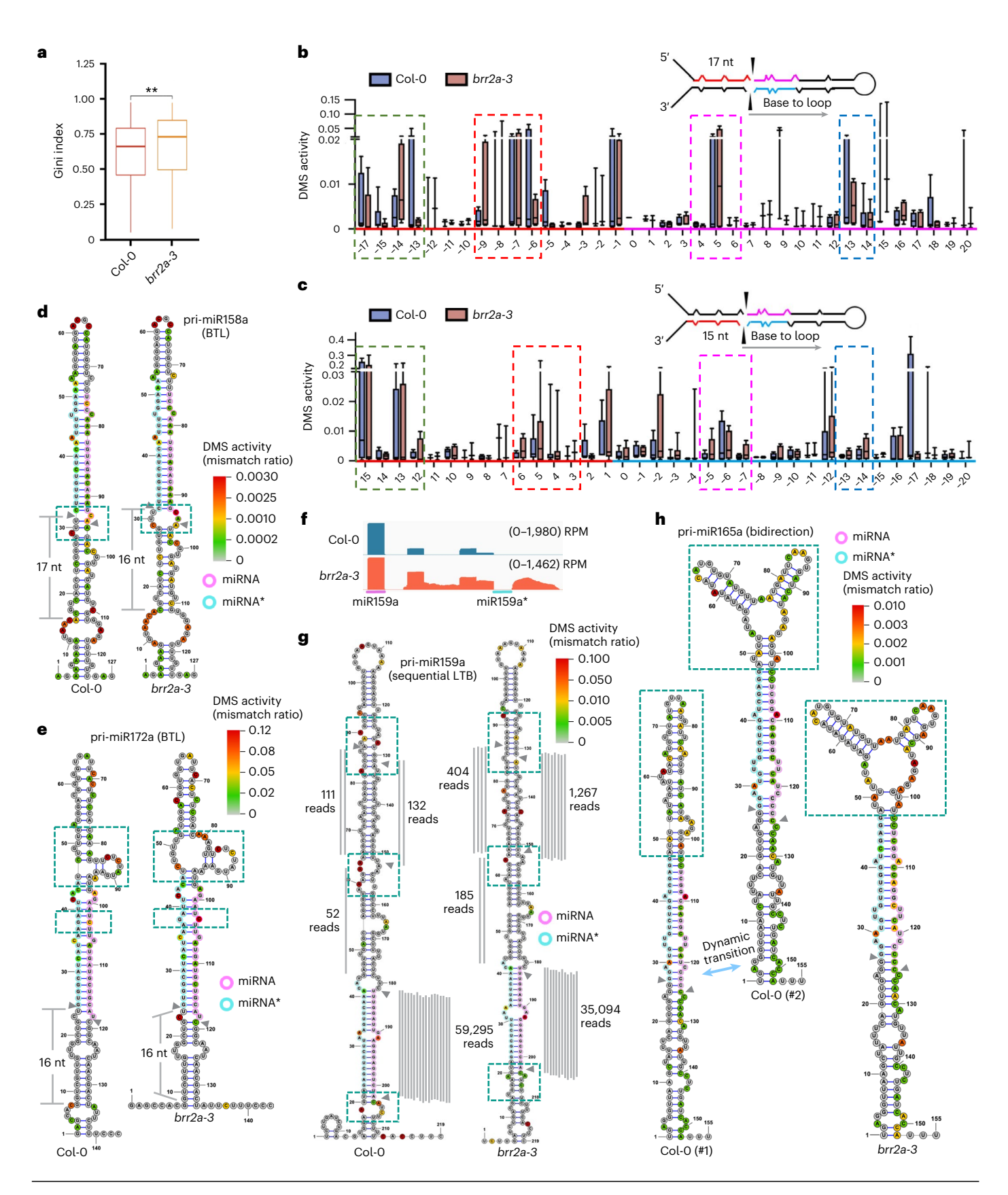
#### Fig. 5 | Brr2a remodels RSS of pri-miRNAs for efficient processing in vivo.

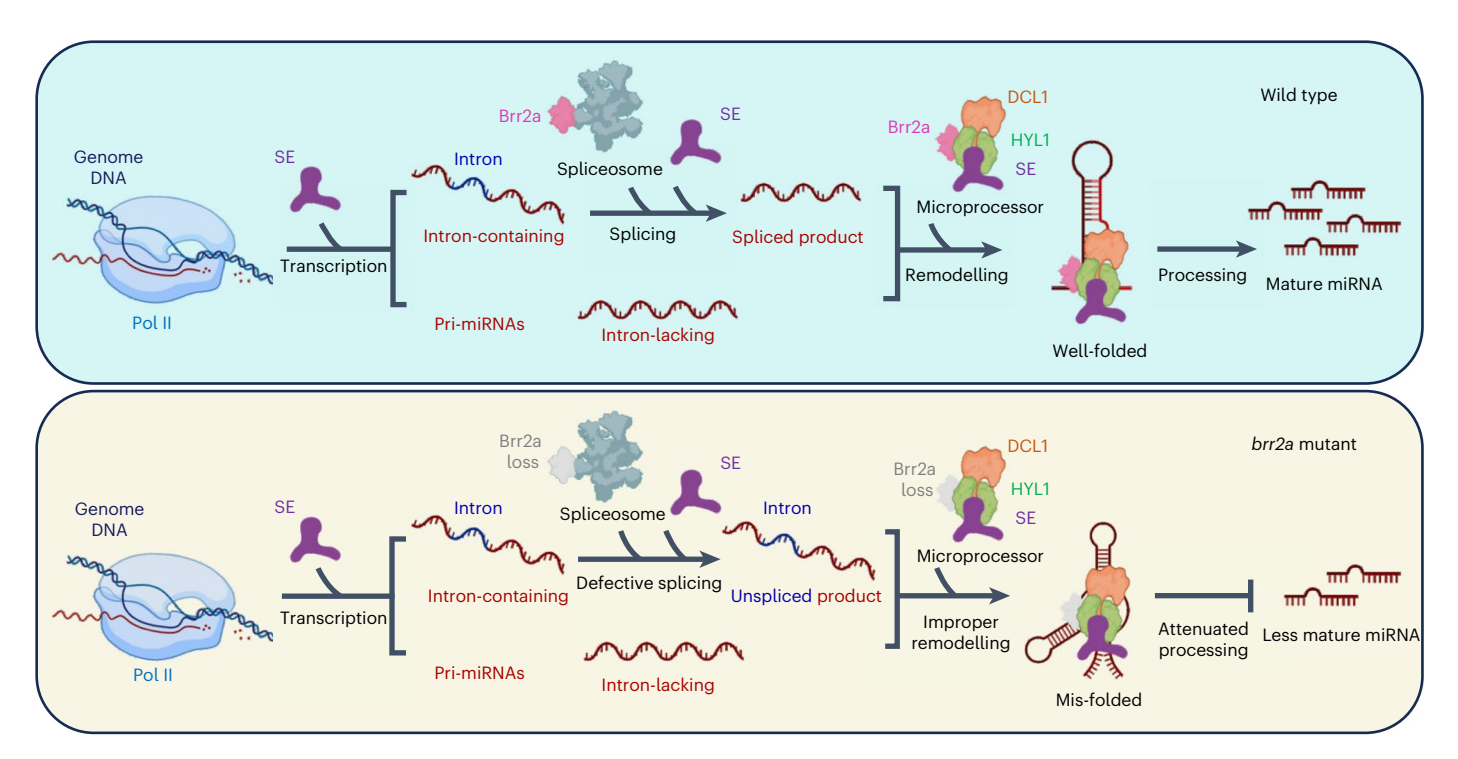
**a**, The Gini index shows an increase in pri-miRNA structural complexity in *brr2a-3* vs Col-0. The Gini index was calculated using sliding windows with a size of 50 nt and a step length of 25 nt. A larger numerical value indicates greater structural complexity. Unpaired two-sided *t*-test; \*\**P* < 0.01. **b**, *c*, Meta profiles show the structural switch at the 5' arm (**b**) and the 3' arm (**c**) of BTL-processed pri-miRNAs in *brr2a-3* vs Col-0. Green dashed boxes, the shifted loops. Red and pink/blue dashed boxes, increased sizes of internal loops at the 5' arm and miRNA/\* duplexes, respectively. In the RNA plot and the *x* axis of the statistical analysis graph, lower stem and miRNA/\* duplex regions are in red and pink/blue, respectively. Position 0 and numbers, the base and the distances to the processing site in the miRNA/\* region. **d**, RSS of pri-miR158a, BTL-typed pri-miRNAs, exhibits structural switch at the first cleavage site in *brr2a-3* vs Col-0. **e**, RSS of pri-miR172a, BTL-typed pri-miRNAs, exhibits structural switch at the upper stem and miRNA/\* duplex regions in *brr2a-3* vs Col-0. **f**, **g**, RSS of

pri-miR159a, LTB-typed pri-miRNAs, exhibits structural switch from the upper stems to the lower stem in brr2a-3 vs Col-0.  $\mathbf{f}$ , the IGV profiles of miR159a in the sRNA-seq, with y axis shown in log scale.  $\mathbf{g}$ , numbers and grey vertical lines are the reads of the major cleavage products of pri-miR159a in Col-0 and brr2a-3 ( $\mathbf{g}$ ).  $\mathbf{h}$ , RSS of pri-miR165a, bidirectionally processed pri-miRNAs, exhibits structural switch at the branched terminal loops in brr2a-3 vs Col-0. The BTL and LTB processing of pri-miR165a produces functional and abortive products, respectively. Two dynamic structures of pri-miR165a in Col-0 are labelled with #1 and #2. Lines, medians; boxes, quartiles; whiskers, minimum to maximum ( $\mathbf{a}$ - $\mathbf{c}$ ). Molecular rulers are indicated in grey ( $\mathbf{d}$  and  $\mathbf{e}$ ). For  $\mathbf{d}$ - $\mathbf{h}$ , pink and blue circles/short lines respectively represent miRNA and miRNA\*; grey arrowheads label the first cutting sites; differences are highlighted by green dashed boxes; DMS activity from high to low is colour coded in a gradient from red to green and grey, as specified in the relevant figure legends.

production, and their mechanisms are interpreted to impact the formation of D-bodies, transcriptional regulation of pri-miRNAs and splicing of the microprocessor components' transcripts. However, whether these proteins have helicase activities and/or whether their functions require the helicase activities are not clear. In contrast,

we demonstrated that Brr2a could hydrolyse ATP and unwind dsRNA in vitro (Fig. 3h,j and Extended Data Fig. 7a). We also showed that Brr2a could reshape plant pri-miRNAs, altering specific structural features in vitro and in vivo (Fig. 5 and Extended Data Fig. 9). Importantly, the ATPase or helicase activity-compromised variants of Brr2a could not





 $\textbf{Fig. 6} \ | \ \textbf{A proposed model of Brr2a function.} \ We \ propose \ a \ model for \ Brr2a \ functions in \ miRNA \ production \ whereby \ Brr2a \ is \ not \ only \ involved \ in \ pri-miRNA \ splicing \ but \ also \ exerts \ helicase \ activity \ to \ modulate \ the \ RSS \ of \ pri-miRNAs, \ thereby \ promoting \ their \ processing.$ 

rescue the miRNA defect in the complementation lines, despite retaining the ability to interact with the microprocessor (Fig. 4d). This underscores the indispensable role of Brr2a's ability to reshape pri-miRNA for efficient production of miRNAs. Thus, Brr2a exhibits a distinct mode of action from other documented RHs in promoting miRNA biogenesis. Importantly, Brr2a's impact on miRNA production is not only limited to intron-containing pri-miRNAs but also to intron-lacking substrates. Nevertheless, Brr2a also mechanistically differs from other reported spliceosome components that regulate miRNA accumulation through their cognate activities in splicing events  $^{6,9-11,43}$ .

The remodelling action of pri-miRNAs by Brr2 seemingly resembles the latter's classical unwinding mechanism of the U4/U6 duplex. The N-helicase cassette of *Arabidopsis* Brr2a, which directly interacts with pri-miRNAs, exhibits both ATPase and helicase activities to reshape RSS<sup>30,34,44</sup>, reminiscent of yeast and human counterparts. Meanwhile, the C-helicase cassette of Brr2a acts as an intramolecular modulator, enhancing the helicase activity of the full-length protein<sup>14</sup>. Notably, there are at least 147 different pri-miRNAs in plants, varying in size from ~100 to several hundred nucleotides, showing heterogeneous shapes and structures<sup>40</sup>. A common feature among all pri-miRNAs is that they carry a stem-loop structure and two flanking single-stranded basal regions. This configuration suggests that the 3' extended single-stranded RNA tail might serve as a docking site for Brr2a, aligning with its canonical model for initial loading onto the ssRNA region of a U4/U6 RNA duplex in the splicing process. In this scenario, Brr2 could reshape the RSS by translocating along pri-miRNAs in a 3' to 5' direction in vivo<sup>14</sup>. For some pri-miRNAs, such as pri-miR396 and pri-miR170 (ref. 40), which have larger internal bulges and loops, respectively, Brr2a might load on these unpaired regions and then translocate along pri-miRNAs. Interestingly, we noticed that Brr2a, different from its human homologue, exhibits a significantly higher affinity to dsRNA vs ssRNA<sup>45</sup>. These results prompted us to hypothesize that Brr2a could directly interact with dsRNA regions of pri-miRNAs and then remodel their structure. However, this hypothesis awaits future testing, ideally via cryo-EM structural analysis of the Brr2a-pri-miRNA complex.

The expression of miRNAs necessitates frequent changes in response to environmental stress and stimuli<sup>3</sup>. Importantly, a growing body of research underscores the pivotal role of RSS in regulating messenger (m)RNA translation, stability, metabolism and other critical processes 46. Pri-miRNAs exhibit sophisticated structures that not only instruct the microprocessor for processing but also contain additional layers of information to be decoded by other RNPs in various physiological contexts. Brr2-mediated remodelling of pri-miRNAs might represent such a novel avenue to reconfigure the pri-miRNA transcriptome for better adaptation to physiological changes. Notably, RSS can be influenced by temperature 46, whereas Brr2, also known as Bad Response to Refrigeration, regulates plants' sensitivity to varying temperatures, as evidenced by mutants displaying a heightened sensitivity to both cold and heat treatments 47-50. A retrospective thought of these findings is that Brr2 might serve as a rapid regulatory switch to finely tune the accumulation of miRNAs, in addition to its canonical role in splicing, in response to both physiological and environmental changes. Finally, the Brr2a protein is highly conserved in eukaryotes, and it would be tempting to learn whether its homologues have a similar function to the Arabidopsis counterpart.

#### Methods

No statistical methods were used to predetermine sample sizes. Randomization and blinding design were not relevant to this study.

#### Plant materials and growth conditions

In this study, *Arabidopsis thaliana* Col-0 ecotype, *hyl1-2* (SALK\_064863) and *se-2* (SAIL\_44\_G12) were used. Col-0 *pMIR159a::FM-GUS* and Col-0 *pMIR159b::FM-GUS* were generated in previous studies<sup>5</sup>. Plants were grown under a 12 h light/12 h dark photoperiod, as previously documented<sup>5</sup>.

To generate brr2a-3, the binary vector of pBA-p35S::amiR-Brr2a was introduced into Col-0. Subsequently, transgenic plants harbouring pBA-p35S::amiR-Brr2a (brr2a-3) were screened for the presence of artificial miRNAs and the reduction in target transcripts in  $T_1$  transgenic

plants, employing sRNA blot analysis and qRT-PCR assays, respectively. To generate *brr2a-2* complementary lines, *pBA-pBrr2a::FM-Brr2a*, *pBA-pBrr2a::FM-Brr2a-E640Q* and *pBA-pBrr2a::FM-Brr2a-S676A T678A* were separately introduced into *brr2a-2* backgrounds using the floral-dip transformation method<sup>51</sup>. T<sub>2</sub> transgenic lines containing FM-tagged Brr2a and its variants were identified through western blot analysis. In addition, *brr2a-2 pBA-pBrr2a::FM-Brr2a* was crossed into *se-2* and *hyl1-2* to obtain *se-2 pBA-pBrr2a::FM-Brr2a* and *hyl1-2 pBA-pBrr2a::FM-Brr2a*. F<sub>3</sub> plants were used for further analysis.

#### Construction of vectors

Most of the cloned coding sequences (CDSs) and genomic DNA sequences were initially introduced into the *pENTR* vector (Invitrogen, A10462) using the primers listed in Supplementary Table 7. Following confirmation through sequencing, they were subsequently cloned into the destination vectors through attL-attR (LR) recombination reactions

The construction of pBA-pBrr2a::FM-gBrr2a, pBA-pBrr2a:: FM-Brr2a, pBA-pBrr2a::FM-Brr2a-EQ and pBA-pBrr2a::FM-Brr2a-AA was carried out as follows: a native promoter containing built-in Xba I and Asc I restriction enzyme cleavage sites, and a Brr2a genomic fragment, were applied using KOD polymerase with Col-0 genomic DNA as a template, along with the primers listed in Supplementary Table 7. The PCR product of the native promoter was cloned into Xba I/Asc I-digested pBA-FM-DC vector to generate pBA-pBrr2a::FM-DC through T4 ligation. The Brr2a genomic fragment was cloned into the pENTR vector, and then an LR reaction was performed with the destination vector pBA-pBrr2a::FM-DC to generate pBA-pBrr2a::FM-gBrr2a. For the mutated variants of Brr2a (EQ and AA), Brr2a cDNA from reverse transcription was cloned into the *pENTR* vector. Subsequently, the catalytically inactive forms were obtained through KOD amplification using the primers listed in Supplementary Table 7. The resulting products, after Dpn I digestion, were transferred into DH5a cells, resulting in pENTR-Brr2a-EQ and pENTR-Brr2a-AA, followed by sequence validation. Subsequently, pBA-pBrr2a::FM-Brr2a, pBA-pBrr2a::FM-Brr2a-EQ and pBA-pBrr2a::FM-Brr2a-AA were constructed through LR reactions.

pET28a-His-SUMO-N-Brr2a, pET28a-His-SUMO-N-EQ, pET28a-His-SUMO-N-AA and pET28a-His-SUMO-C-Brr2a were constructed as follows: the N-Brr2a (487 to 1,288 aa) and C-Brr2a (1,289 to 2,171 aa) fragments, each containing built-in BamH I and Sal I sites, were amplified using pENTR-Brr2a as the template and the primers listed in Supplementary Table 7. Similarly, the N-Brr2a-EQ and N-Brr2a-AA fragments were also amplified using pENTR-Brr2a-EQ and pENTR-Brr2a-AA as the template, respectively, and the primers listed in Supplementary Table 7. The PCR fragments of N-Brr2a, N-Brr2a-EQ, N-Brr2a-AA and C-Brr2a were cloned into BamH I/Sal I-digested pET28a-His-SUMO to generate final vectors, including pET28a-His-SUMO-N-Brr2a-AA and pET28a-His-SUMO-N-Brr2a-EQ, pET28a-His-SUMO-N-Brr2a-AA and pET28a-His-SUMO-C-Brr2a.

#### Co-IP assay

Co-immunoprecipitation was conducted in 3-week-old *Arabidopsis* plants. Total proteins were extracted from 0.2 g of finely ground powder using 1 ml of IP buffer (comprising 40 mM Tris-HCl pH 7.5, 150 mM NaCl, 5 mM MgCl<sub>2</sub>, 5 mM dithiothreitol (DTT), 0.5% Triton X-100,2% glycerol,1 mM phenylmethyl sulfonyl fluoride (PMSF),50  $\mu$ M MG-132 and 1 pellet per 10 ml of Complete EDTA-free protease inhibitor from Roche). Subsequently, protein extracts were subjected to immunoprecipitation using anti-Flag M2 magnetic beads (Sigma-Aldrich, M8823) at 4 °C for 2 h. For RNase treatment, 50  $\mu$ l of RNase A (1 mg ml $^{-1}$ ) (Thermo Fisher, EN0531) was introduced into 1 ml of the immunoprecipitation buffer during the incubation period. After the incubation, the beads were washed four times with IP buffer at 4 °C for 5 min each, followed by the application of SDS loading buffer at 95 °C for 10 min.

#### RIP and ChIP assays

RIP and ChIP assays were conducted following established procedures<sup>32</sup>. The brr2a-2 pBrr2a::FM-Brr2a was crossed with se-2 and hyl1-2 to switch genetic backgrounds. The Brr2a variant transgenic plants were generated by complementing brr2a-2 with pBrr2a::FM-Brr2a-variants. Three-week-old seedlings were crosslinked using the buffer (20 mM HEPES pH7.4,1 mM PMSF,1 mM EDTA, 0.4 M sucrose, 1% formaldehyde) and ground to fine powder. Plant nuclei were isolated from 2 g or 3 g plant powder and resuspended with nuclei sonication buffer (40 mM Tris-HCl pH 7.4, 150 mM NaCl, 5 mM MgCl<sub>2</sub>, 1% SDS, 1 mM DTT, 1% Triton X-100, 2% glycerol, 1 mM PMSF, 50 µM MG-132, and 1 pellet per 10 ml complete EDTA-free protease inhibitor and 10 U SUPERase-In RNase inhibitor (Thermo Fisher)) for sonication (15 cycles, 30 s sonication and 90 s pause). The supernatant was diluted 9 times with dilution buffer (40 mM Tris-HClpH7.4,150 mM NaCl, 5 mM MgCl<sub>2</sub>,1 mM DTT, 2% glycerol, 1 mM PMSF, 50 µM MG-132, 1 pellet per 10 ml complete EDTA-free protease inhibitor and 10 U ml<sup>-1</sup>SUPERase-In RNase inhibitor). Either Flag antibodies or endogenous antibodies of NRPB2 (PhytoAB, PHY2429S) were used for RIP or ChIP, respectively. The immunoprecipitations were performed at 4 °C with agitation for 2 h (RIP) or overnight (ChIP). IP samples were washed with dilution buffer, high salt wash buffer (20 mM Tris-HCl pH 7.4, 500 mM NaCl, 5 mM MgCl<sub>2</sub>, 50 µM ZnCl<sub>2</sub>, 1 mM DTT, 1 mM PMSF, 0.5% Triton X-100, 50 µM MG-132,1 pellet per 10 ml complete EDTA-free protease inhibitor and 10 U ml<sup>-1</sup> SUPERase-In RNase Inhibitor), LiCl wash buffer (0.25 MLiCl, 1% NP-40, 1% sodium deoxycholate, 20 mM Tris-HCl pH 7.4, 1 mM EDTA) and Proteinase K buffer (20 mM Tris-HCl pH 7.4, 200 mM NaCl and 10 U SUPERase-In RNase inhibitor). RNA or DNA was eluted from de-crosslinking with Proteinase K solution (20 mM Tris-HCl pH 7.4, 200 mM NaCl, 1 mg ml<sup>-1</sup> Proteinase K, 1% SDS and 10 U SUPERase-In RNase inhibitor, 10 mM EDTA) on a Thermomixer shaker at 65 °C for 2 h or 6 h, respectively. Following this, RNA underwent purification using RNA Clean & Concentrator kits (ZYMO, R1017) and was treated with  $DN as ebefore\,RT-qPCR\,analysis.\,DNA\,underwent\,RN as etreatment\,and$ subsequent purification using DNA Clean & Concentrator kits (ZYMO, D4004). For Pol II ChIP in brr2a mutants vs Col-0 and Brr2a RIP in hyl1-2 pBrr2a::FM-Brr2avs se-2 pBrr2a::FM-Brr2a, quantification was performed by first normalizing the amount from IP to the input and then to that of the Col-0 and se-2 pBrr2a::FM-Brr2a which were arbitrarily set as 1 for both ChIP and the RIP assays. For the RIP of Brr2a and its variants, quantification was performed by normalizing the amount of Brr2a variant IP-derived RNA to that of the immunoprecipitated proteins and then to that of wild-type Brr2a where the ratio was arbitrarily set as 1.

#### **BiFC** assay

Tobacco plants were used for BiFC assays<sup>26</sup>. Briefly, *p35S::nYFP-Brr2a* was co-infiltrated with *p35S::cYFP-HYL1*, *p35S::cYFP-SE* and *p35S::cYFP-DCL1* in the leaves of 4-week-old tobacco plants. The fluorescence signals were detected 3 days later. YFP fluorescence signals were excited at 514 nm. The emissions for YFP and chlorophyll fluorescence are 525–550 nm and 661–700 nm, respectively. All images were acquired using a Leica stellaris 5 laser-scanning confocal microscope with LAS X Life Science microscope software.

#### RNA and sRNA sequencing and bioinformatics

Total RNA for RNA-seq and sRNA-seq was extracted from 3-week-old soil-grown plants of Col-0 and the *brr2a* mutants using TRI reagent (Sigma). Library preparation and analysis for RNA-seq and sRNA-seq using Illumina sequencing followed established protocols<sup>26</sup>. DESeq2 analysis was used for normalization in RNA-seq. Reads per million (RPM) of miRNAs were counted and normalized on the basis of the amount of sRNAs that were derived from rRNA.

#### RT-qPCR

Genomic DNA was removed by DNase before reverse transcription. Random hexamers and oligo(dT)<sub>12-18</sub> were used to detect mRNA and

pri-miRNAs. Primers and procedures of stem-loop qPCR detecting miRNA expression were adopted from a previous study<sup>26</sup>. Relative expression level was calculated with the  $2^{-\Delta\Delta Ct}$  method.

#### sRNA blot

The sRNA blot assays were conducted on 10-day-old seedlings using the primers listed in Supplementary Table 7, following an established method adopted from a previous study  $^{39}$ . Total RNA was extracted using TRI reagent (Sigma-aldrich, T9424) and Turbo DNase treatment (2 U Turbo DNase per 50  $\mu g$  of RNA) (Invitrogen, AM2239). Urea-polyacrylamide gels (15%) were used to separated RNA samples. Following electrophoresis, RNA was transferred onto a nylon membrane (GE Healthcare) using a semi-dry transfer apparatus. The sRNA and U6 probes were labelled using  $[\gamma^{-32}P]$  ATP with T4 PNK and 21-nucleotide DNA oligos that are complementary to the corresponding sequences. Signals were detected with a Typhoon FLA7000 imaging system (GE Healthcare). The stripped membrane was then rehybridized with a different sRNA and U6 probes following the same hybridization and washing procedures.

#### Western blot

The blots were probed with specific antibodies as follows: actin (Sigma-Aldrich, A0480), NRPB2 (PhytoAB, PHY2429S), HSP70 (Agrisera, AS08371), MYC (Sigma, C3956), HYL1 (homemade), DCL1 (Agrisera, AS122102), AGO1 (Agrisera, AS09527) and SE (homemade). Secondary antibodies used in this study were anti-rabbit (GE Healthcare, NA934) and anti-mouse IgG (GE Healthcare, NA931).

#### **GUS** staining

Staining assays were carried out using the  $F_3$  generation of *pMIR159a*::*FM-GUS* and *pMIR159b*::*FM-GUS* in either Col-0 or *brr2a-3* background. For each sample, tissues were collected from at least 10 individual plants. The plant tissues were incubated in GUS staining solution (120 mM  $Na_2HPO_4$ , 78 mM  $NaH_2PO_4$ , 2 mM potassium ferricyanide [ $K_3Fe(CN)_6$ ], 2 mM potassium ferrocyanide [ $K_4Fe(CN)_6$ ], 0.1% Triton X-100, 10 mM EDTA, 10% methanol and 2 mM X-Gluc (Thermo Fisher, R0851)) at 37 °C overnight<sup>26</sup>. After staining, the tissues were cleared with 70% ethanol to remove chlorophyll at 37 °C overnight with a horizontal shaker. GUS expression patterns were documented using a stereo microscope.

#### Expression and purification of recombinant proteins

To purify recombinant truncated Brr2a and its variants from *E. coli*, BL21 (DE3) cells carrying plasmid were grown in Luria Broth (LB) medium at 37 °C until optical density (OD)  $_{600}$  = 0.6. Recombinant protein expression was induced with 0.5 mM isopropyl- $\beta$ -D-thiogalactopyranoside at 16 °C overnight. Then, bacterial cells were collected and resuspended in a lysis buffer that contained the following components: 40 mM Tris-HCl pH 8.0, 800 mM NaCl, 2% glycerol, 5 mM  $\beta$ -mercaptoethanol, 3 mM PMSF, 0.5% Triton X-100, 50  $\mu$ M MG-132 and 1 pellet of complete EDTA-free protease inhibitor (Roche) per 50 ml of buffer. The resuspended cells were then disrupted using a high-pressure homogenizer (Microfluidics). Following cell disruption, the lysate was clarified through a combination of centrifugation (21,000 × g at 4 °C for 30 min) and filtration via a 0.4  $\mu$ m filter. The cleared lysate was supplemented with imidazole to a final concentration of 20 mM. Finally, the prepared lysate was loaded onto a HisTrap HP column (GE Healthcare, 17524802).

The column was initially washed with 25 ml of a wash buffer composed of 40 mM Tris-HCl at pH 8.0, 800 mM NaCl, 2% glycerol and 20 mM imidazole. Subsequently, elution was carried out using a gradient elution buffer ranging from 20 to 300 mM imidazole. Peak fractions containing the recombinant truncated Brr2a or its variants were combined and concentrated using a 50 kDa molecular weight cut-off (MWCO) centricon (Millipore). The concentrated sample was then loaded onto a HiLoad 16/600 Superdex 200 pg column (GE Healthcare).

The gel filtration buffer for the Superdex column consisted of 20 mM Tris-HCl pH 8.0 and 500 mM NaCl. Peak fractions containing Brr2a or its variants were collected and subsequently dialysed with 11 of dialysis buffer (10 mM Tris-HCl at pH 8.0, 150 mM NaCl, 30% glycerol and 1 mM  $\beta$ -mercaptoethanol) at 4 °C for 6 h. The final purified protein was quantified using SDS-PAGE and then divided into aliquots for storage at –80 °C.

#### **EMSA**

EMSA was conducted as previously described<sup>5</sup>. In summary, recombinant Brr2a or its variants were mixed with labelled pri-miRNA or ssRNA in the EMSA buffer, consisting of 20 mM Tris-HCl (pH 8.0), 150 mM NaCl and 10% glycerol. The mixtures were incubated at room temperature for 30 min and then separated on a native 1% agarose gel. The images were quantified with ImageJ. Prism 9 (GraphPad) was used to calculate  $K_d$  and app $K_d$  with a Hill slope model.

#### ATPase assay

The procedure for the ATPase assay was adapted from a previously described method  $^5$ . Fresh purified recombinant Brr2a or its variants at the respective concentrations were introduced into ATP hydrolysis reactions (10 µl) comprising 20 mM Tris-HCl pH 8.0, 150 mM NaCl, 5 mM MgCl<sub>2</sub>, 12% glycerol, 2 mM DTT and 750 ng of folded pri-miR159b. The above mixture was pre-incubated for 10 min before the addition of 1 mM cold ATP and 0.1 µl [ $\gamma^{-32}$ P] ATP (PerkinElmer, 6,000 Ci mmol $^{-1}$ ). Reactions were incubated at 37 °C for the specified time intervals and then terminated by loading the samples onto a polyethyleneimine-cellulose (PEI-cellulose) TLC plate. The plate was developed in 0.5 MLiCl and 1 M formic acid. Liberated phosphate was analysed through TLC and phosphor imaging.

#### RNA remodelling assay

The unwinding assay was conducted with slight modifications to a previously published method<sup>52</sup>. Three dsRNA duplexes were made: (1) pri-miR159b duplex with a ~20-nt over-hung single-stranded RNA and a stem-loop on its 3' end, (2) nicked pri-miR166f duplex with one nucleotide gap and (3) a model dsRNA duplex with a ~110 nt 3' overhang. The duplexed dsRNAs were generated by co-folding long cold RNA and short hot RNA in vitro. The final purified RNAs were visualized through native PAGE gels to observe released short RNA and dsRNA that remained annealed. Freshly purified truncated Brr2a and its variants from E. coli, and freshly immunoprecipitated full-length Brr2a and its variant proteins from plants were used. Plant Brr2a and its variants were immunoprecipitated from transgenic plants of brr2a-2 pBA-pBrr2a::FM-Brr2a, brr2a-2 pBA-pBrr2a::FM-Brr2a-EQ and brr2a-2 pBA-pBrr2a::FM-Brr2a-AA, respectively, using M2 beads. Subsequently, the resulting beads were washed with the IP buffer and high salt buffer (comprising 40 mM Tris-HCl pH 7.5, 500 mM NaCl, 0.5% NP-40, 1 mM PMSF, 50 μM MG-132, 0.2 U μl<sup>-1</sup> SUPERase-In RNase inhibitor and 1 pellet per 10 ml of complete EDTA-free protease inhibitor from Roche) for three times each. Each washing step included 5 min agitation at 4 °C for 5 min. Proteins were eluted using Flag peptide (Sigma-Aldrich, F4799). The eluate was detected by western blot before unwinding assays.

To prepare the pri-miRNA substrates, the indicated 5'- $^{32}$ P-labelled short RNA fragment was hybridized with a truncated strand of pri-miR166f, pri-miR159b and LUC reverse. Annealed RNA duplexes were purified by native polyacrylamide gel electrophoresis (native PAGE). Subsequently, 200 nM recombinant proteins or freshly immunoprecipitated Brr2a or its variants were mixed with the RNA duplexes (5 fmol, signalling 500–2,000 c.p.m. per reaction) in a remodelling buffer containing 40 mM Tris-HCl pH 8.0, 75 mM NaCl, 1.5 mM DTT, 100 ng  $\mu$ l<sup>-1</sup> acetylated BSA and 8% glycerol at room temperature for 10 min allowing RNP formation. Reactions were started by adding 5 mM MgCl<sub>2</sub> and 10 mM ATP per 1 mM GTP. The reaction mixtures were incubated at 25 °C for the specified time course and halted by adding 800 mM NaCl (to elute RNA from proteins) and 0.1 M of cold short RNA

fragment (to prevent re-annealing). The mixtures were then subjected to phenol-chloroform-isoamyl alcohol purification. Following this, the RNA samples were separated using 12% native PAGE gels and the signals were visualized through radiography. Quantification of the results was performed using ImageJ (GE Healthcare).

#### Target-specific DMS-MaPseq library preparation

DMS-MaPseq for pri-miRNAs was performed as described with modification<sup>5,39,40</sup>. Briefly, total RNA was extracted from 3-week-old plants after treatment with 1% DMS. RNA was then subjected to DNase treatment and rRNA depleted. The resulting RNA was mixed with dNTP and gene-specific primers (20 pmol per primer, up to 20 gene-specific primers in one reaction; see oligo information in Supplementary Table 7) and incubated at 65 °C for 5 min. Following this, 4 µl of 5× First-Strand buffer (250 mM Tris-HCl pH 8.3, 375 mM KCl, 15 mM MgCl<sub>2</sub>), 1 μl of 0.1 M DTT, 1 μl of RNase inhibitor and 1 μl of TGIRT-III (InGex) were added. Reverse transcription was carried out at 42 °C for 30 min and then at 60 °C for 1.5 h. The reaction was terminated by adding 2 µl of 2.5 M NaOH and heating at 95 °C for 15 min. After neutralization with 5 M HCl, the mixture was purified using RNAClean XP beads (Beckman) to remove RT primers and nucleotides. Subsequently, pri-miRNAs were amplified using KOD hot start DNA polymerase (Millipore) with gene-specific primers (Supplementary Table 7) and the above-mentioned cDNA as a template. PCR bands were cut from the gel, purified by AMPure XP beads (Beckman) and normalized on the basis of their band intensities before library construction. Subsequently, the PCR fragments underwent end repair, adenylation and adaptor ligation using Illumina adapters, primarily following published protocol<sup>39</sup>. The fragments were barcoded through adaptor ligation and the ligation products purified using AMPure XP beads. Next, the purified barcoded libraries were enriched through 10 cycles of PCR using KOD hot start DNA polymerase. Finally, the PCR products were cleaned using AMPure XP beads. Before sequencing, the libraries were quantified using the Agilent TapeStation system and then subjected to 150 bp single-end reads sequencing on the Illumina NextSeq 500 platform.

#### Analysis of DMS-MaPseq

DMS-MaPseq was conducted for individual pri-miRNAs following the procedure with modified analysis 5,39,40. In summary, raw fastq files underwent an initial quality control filter, necessitating a quality score >25 at the 3' end and subsequently trimmed to eliminate adaptor sequences using Cutadapt. To ensure the attainment of high sequence quality, we employed 'Fastq\_quality\_filter' of the 'Fastx-toolkit' (Fastx-toolkit, https://github.com/agordon/fastx toolkit), applying the parameters '-q 25-p80'. This configuration mandated that 80% of nucleotides exhibit a base call accuracy exceeding 99.7%, thereby filtering out reads with low quality. For the retained reads of high quality over 50 nt, we proceeded to map them to the *Arabidopsis* Araport11 genome using tophat2, incorporating the following parameters: '-N 15 -read-gap-length 10 -read-edit-dist 15 max-insertion-length 5 -max-deletion-length 5 -g 3'. Only reads with unique mapping were retained for the identification of mismatches. The identification of mismatches was carried out using a custom Python script named 'CountMismatch2Bed.py' (https://github. com/changhaoli/TAMU\_02RSS) as in a previous study<sup>40</sup>. DMS reactivity was determined by computing the ratio of mismatch counts to the total read counts for individual nucleotides. The average mismatch ratios, encompassing A/C/G/U, were calculated and plotted on a bar plot using the R package 'ggpubr' (ggpubr: 'ggplot2' based publication-ready plots; https://cran.r-project.org/web/packages/ggpubr/index.html). The Gini index was calculated as previously described<sup>53</sup>.

#### Visualization of pri-miRNA secondary structure models

Folding of pri-miRNA secondary structure in vivo was based on the constraints from DMS-MaPseq signals following previously described procedures  $^{40,53}$ . To better distinguish the changes in DMS modification

levels between Col-0 and brr2a-3, DMS activity from high to low were colour coded in a gradient from red to green for each target pri-miRNA. Adenine and cytosine bases with an in vitro radiometric signal greater than the selected threshold, varying between 0.09 and 0.0025, as specified in the relevant figure legends, were required to be unpaired. On the basis of miRBase annotation, all mature miRNA sequences were outlined in pink, while miRNA\* sequences were outlined in blue.

#### **Graph drawing**

Graphs with dot plots (individual data points) were drawn using Graph-Pad Prism 9. Models and illustrations were created with BioRender.com.

#### Statistics and reproducibility

Statistical analyses of quantification results were performed using GraphPad Prism 9. Statistical data show the mean  $\pm$  s.d. or  $\pm$  s.e. of at least 3 biologically independent experiments or samples as described in figure legends. Two-tailed unpaired t-test, one-way and two-way analysis of variance (ANOVA) with Dunnett's multiple comparisons test, and two-way ANOVA were performed in Graphpad Prism 9. The hypergeometric distribution test was conducted in R. No statistical method was used to predetermine sample size, which was determined in accordance with previous studies 5.26,54 and standard practices in the field. All experiments were independently repeated more than three times with similar results obtained, and the exact replicate numbers are provided in the respective figure legends. No data were excluded from our studies. Plants were randomly assigned to experimental groups whenever possible. For other experiments, the experiments were randomized and the investigators were blinded to allocation.

#### **Reporting summary**

Further information on research design is available in the Nature Portfolio Reporting Summary linked to this article.

#### **Data availability**

The Col-O control for RNA-seq and sRNA-Seq and the Col-O control for DMS-MaPseq were adopted from the PRJNA613247 and PRJNA1092576 studies, respectively, since the sequence libraries of brr2a mutants were prepared simultaneously. Data generated in this study can be accessed under accession number PRJNA1117818 in the NCBI BioProject database (https://www.ncbi.nlm.nih.gov/bioproject/1117818). For the convenience of readers, we have also uploaded the original data for the control groups. In addition, genetic materials will be made available upon request. RNA-seq<sup>25</sup> and sRNA-seq<sup>27</sup> data of hyl1-2 can be accessed under accession numbers PRJNA116651 in the NCBI Bio-Project database (https://www.ncbi.nlm.nih.gov/bioproject/?term= PRJNA116651) and GSE111814 in the NCBI GEO database (https://www. ncbi.nlm.nih.gov/geo/query/acc.cgi?acc=GSE111814), respectively. RNA-seq data of se-2 (ref. 26) can be accessed under accession number PRJNA613247 in the NCBI BioProject database (https://www.ncbi.nlm. nih.gov/bioproject/613247). The pan-transcriptome was re-analysed from the dataset adopted from a previous study<sup>47</sup>. Source data are provided with this paper.

#### **Code availability**

This paper does not report original code.

#### References

- Bohnsack, K. E., Yi, S., Venus, S., Jankowsky, E. & Bohnsack, M. T. Cellular functions of eukaryotic RNA helicases and their links to human diseases. *Nat. Rev. Mol. Cell Biol.* 24, 749–769 (2023).
- 2. Xu, Y. & Chen, X. microRNA biogenesis and stabilization in plants. *Fundam. Res.* **3**, 707–717 (2023).
- Song, X., Li, Y., Cao, X. & Qi, Y. MicroRNAs and their regulatory roles in plant-environment interactions. *Annu. Rev. Plant Biol.* 70, 489–525 (2019).

- Zhu, H. et al. Bidirectional processing of pri-miRNAs with branched terminal loops by *Arabidopsis* Dicer-like1. *Nat. Struct. Mol. Biol.* 20, 1106–1115 (2013).
- Wang, Z. et al. SWI2/SNF2 ATPase CHR2 remodels pri-miRNAs via Serrate to impede miRNA production. Nature 557, 516–521 (2018).
- Knop, K. et al. Active 5' splice sites regulate the biogenesis efficiency of Arabidopsis microRNAs derived from intron-containing genes. Nucleic Acids Res. 45, 2757–2775 (2017).
- Zielezinski, A. et al. mirEX 2.0 an integrated environment for expression profiling of plant microRNAs. BMC Plant Biol. 15, 144 (2015).
- Stepien, A. et al. Chromatin-associated microprocessor assembly is regulated by the U1 snRNP auxiliary protein PRP40. *Plant Cell* 34, 4920–4935 (2022).
- Li, M. et al. Serrate-Associated Protein 1, a splicing-related protein, promotes miRNA biogenesis in *Arabidopsis*. New Phytol. 232, 1959–1973 (2021).
- Fan, L. et al. Arabidopsis AAR2, a conserved splicing factor in eukaryotes, acts in microRNA biogenesis. Proc. Natl Acad. Sci. USA 119, e2208415119 (2022).
- Xiong, F. et al. Arabidopsis JANUS regulates embryonic pattern formation through Pol II-mediated transcription of WOX2 and PIN7. iScience 19, 1179–1188 (2019).
- Yan, C., Wan, R. & Shi, Y. Molecular mechanisms of pre-mRNA splicing through structural biology of the spliceosome. *Cold Spring Harb. Perspect. Biol.* 11, a032409 (2019).
- 13. Li, X. et al. Functions and mechanisms of RNA helicases in plants. J. Exp. Bot. **74**, 2295–2310 (2023).
- Santos, K. F. et al. Structural basis for functional cooperation between tandem helicase cassettes in Brr2-mediated remodeling of the spliceosome. *Proc. Natl Acad. Sci. USA* 109, 17418–17423 (2012).
- Pause, A. & Sonenberg, N. Mutational analysis of a DEAD box RNA helicase: the mammalian translation initiation factor eIF-4A. EMBO J. 11, 2643–2654 (1992).
- Sloan, K. E. & Bohnsack, M. T. Unravelling the mechanisms of RNA helicase regulation. *Trends Biochem. Sci.* 43, 237–250 (2018).
- Jia, T. et al. The Arabidopsis MOS4-associated complex promotes MicroRNA biogenesis and precursor messenger RNA splicing. Plant Cell 29, 2626–2643 (2017).
- Bajczyk, M. et al. SERRATE interacts with the nuclear exosome targeting (NEXT) complex to degrade primary miRNA precursors in *Arabidopsis*. *Nucleic Acids Res.* 48, 6839–6854 (2020).
- Kurihara, Y. & Watanabe, Y. Arabidopsis micro-RNA biogenesis through Dicer-like 1 protein functions. Proc. Natl Acad. Sci. USA 101, 12753–12758 (2004).
- 20. Li, Q. et al. DEAD-box helicases modulate dicing body formation in *Arabidopsis*. Sci. Adv. **7**, eabc6266 (2021).
- 21. He, B. et al. RNA-binding proteins contribute to small RNA loading in plant extracellular vesicles. *Nat. Plants* **7**, 342–352 (2021).
- Wei, X. et al. Structural basis of microRNA processing by Dicer-like 1. Nat. Plants 7, 1389–1396 (2021).
- 23. Mahrez, W. et al. BRR2a affects flowering time via FLC splicing. *PLoS Genet.* **12**, e1005924 (2016).
- Schwab, R., Ossowski, S., Riester, M., Warthmann, N. & Weigel, D. Highly specific gene silencing by artificial microRNAs in *Arabidopsis*. *Plant Cell* 18, 1121–1133 (2006).
- Kurihara, Y. et al. Transcriptome analyses revealed diverse expression changes in ago1 and hyl1 *Arabidopsis* mutants. *Plant Cell Physiol.* 50, 1715–1720 (2009).
- Li, Y. et al. Degradation of SERRATE via ubiquitin-independent 20S proteasome to survey RNA metabolism. *Nat. Plants* 6, 970–982 (2020).
- Ma, Z. et al. Arabidopsis Serrate coordinates histone methyltransferases ATXR5/6 and RNA processing factor RDR6 to regulate transposon expression. Dev. Cell 45, 769–784.e6 (2018).

- Laubinger, S. et al. Dual roles of the nuclear cap-binding complex and SERRATE in pre-mRNA splicing and microRNA processing in Arabidopsis thaliana. Proc. Natl Acad. Sci. USA 105, 8795–8800 (2008).
- 29. Li, S. et al. SMA1, a homolog of the splicing factor Prp28, has a multifaceted role in miRNA biogenesis in *Arabidopsis*. *Nucleic Acids Res.* **46**, 9148–9159 (2018).
- Mozaffari-Jovin, S. et al. The Prp8 RNase H-like domain inhibits Brr2-mediated U4/U6 snRNA unwinding by blocking Brr2 loading onto the U4 snRNA. Genes Dev. 26, 2422–2434 (2012).
- 31. Hahn, D., Kudla, G., Tollervey, D. & Beggs, J. D. Brr2p-mediated conformational rearrangements in the spliceosome during activation and substrate repositioning. *Genes Dev.* **26**, 2408–2421 (2012).
- Zhong, S. et al. Anaphase-promoting complex/cyclosome regulates RdDM activity by degrading DMS3 in *Arabidopsis*. Proc. Natl Acad. Sci. USA 116, 3899–3908 (2019).
- Luders, J. et al. Identification of pri-miRNA stem-loop interacting proteins in plants using a modified version of the Csy4 CRISPR endonuclease. *Int. J. Mol. Sci.* 23, 8961 (2022).
- Zhang, L. et al. Structural evidence for consecutive Hel308-like modules in the spliceosomal ATPase Brr2. Nat. Struct. Mol. Biol. 16, 731–739 (2009).
- Pause, A. & Sonenberg, N. Mutational analysis of a DEAD box RNA helicase: the mammalian translation initiation factor eIF-4A. EMBO J. 11, 2643–2654 (1992).
- 36. Story, R. M., Li, H. & Abelson, J. N. Crystal structure of a DEAD box protein from the hyperthermophile *Methanococcus jannaschii*. *Proc. Natl Acad. Sci. USA* **98**, 1465–1470 (2001).
- 37. Nguyen, T. H. et al. The architecture of the spliceosomal U4/U6.U5 tri-snRNP. *Nature* **523**, 47–52 (2015).
- 38. Sun, D. et al. The epigenetic factor FVE orchestrates cytoplasmic SGS3-DRB4-DCL4 activities to promote transgene silencing in *Arabidopsis*. Sci. Adv. **7**, eabf3898 (2021).
- 39. Wang, Z., Wang, M., Wang, T., Zhang, Y. & Zhang, X. Genome-wide probing RNA structure with the modified DMS-MaPseq in *Arabidopsis*. *Methods* **155**, 30–40 (2019).
- 40. Yan, X. et al. Parallel degradome-seq and DMS-MaPseq substantially revise the miRNA biogenesis atlas in *Arabidopsis*. *Nat. Plants* **10**, 1126–1143 (2024).
- Bologna, N. G., Mateos, J. L., Bresso, E. G. & Palatnik, J. F. A loop-to-base processing mechanism underlies the biogenesis of plant microRNAs miR319 and miR159. EMBO J. 28, 3646–3656 (2009).
- 42. Gu, S. et al. The loop position of shRNAs and pre-miRNAs is critical for the accuracy of dicer processing in vivo. *Cell* **151**, 900–911 (2012).
- Wang, J. et al. Spliceosome disassembly factors ILP1 and NTR1 promote miRNA biogenesis in *Arabidopsis thaliana*. *Nucleic Acids* Res. 47, 7886–7900 (2019).
- Absmeier, E. et al. The large N-terminal region of the Brr2 RNA helicase guides productive spliceosome activation. *Genes Dev.* 29, 2576–2587 (2015).
- Absmeier, E., Becke, C., Wollenhaupt, J., Santos, K. F. & Wahl, M. C. Interplay of cis- and trans-regulatory mechanisms in the spliceosomal RNA helicase Brr2. Cell Cycle 16, 100–112 (2017).
- 46. Zhu, J., Li, C., Peng, X. & Zhang, X. RNA architecture influences plant biology. *J. Exp. Bot.* **72**, 4144–4160 (2021).
- Zhang, H. et al. A comprehensive online database for exploring-20,000 public *Arabidopsis* RNA-seq libraries. *Mol. Plant* 13, 1231–1233 (2020).
- 48. Pietzenuk, B. et al. Recurrent evolution of heat-responsiveness in Brassicaceae COPIA elements. *Genome Biol.* 17, 209 (2016).
- Sato, H., Suzuki, T., Takahashi, F., Shinozaki, K. & Yamaguchi-Shinozaki, K. NF-YB2 and NF-YB3 have functionally diverged and differentially induce drought and heat stress-specific genes. *Plant Physiol.* 180, 1677–1690 (2019).

- Klepikova, A. V., Kulakovskiy, I. V., Kasianov, A. S., Logacheva, M. D. & Penin, A. A. An update to database TraVA: organ-specific cold stress response in *Arabidopsis thaliana*. *BMC Plant Biol.* 19, 29–40 (2019).
- 51. Zhang, X., Henriques, R., Lin, S.-S., Niu, Q.-W. & Chua, N.-H. *Agrobacterium*-mediated transformation of *Arabidopsis thaliana* using the floral dip method. *Nat. Protoc.* **1**, 641–646 (2006).
- 52. Valentini, M. & Linder, P. in RNA Remodeling Proteins. Methods in Molecular Biology Vol. 2209 (ed. Boudvillain, M.) 17–34 (Humana, 2021).
- Zubradt, M. et al. DMS-MaPseq for genome-wide or targeted RNA structure probing in vivo. Nat. Methods 14, 75–82 (2017).
- 54. Xie, D. et al. Phase separation of SERRATE drives dicing body assembly and promotes miRNA processing in *Arabidopsis*. *Nat. Cell Biol.* **23**, 32–39 (2021).

#### Acknowledgements

We thank L. Hennig for the cäö (brr2a-2) seeds, all the members of the Zhang Laboratory for their help and careful proofreading of this manuscript, and the TAMU HPRC (High Performance Research Computing) group for supercomputing support. The work was supported by grants from NIH R35GM151976, NSF MCB 2139857 and Welch Foundation A-2177-20230405 to X.Z.

#### **Author contributions**

X.Z. and S.Z. conceived the project. X.Z., X.L. and S.Z. designed the experiments. X.L. and S.Z. performed most of the experiments. C.L. analysed sequencing data. X.Y. and J.Z. participated in DMS-MaPseq library preparation. Y.L. performed sRNA-seq. Z.W. generated the *brr2a-3* transgenic plants. X.P. provided intellectual and experimental support. X.L. and S.Z. wrote the initial draft of the manuscript and X.Z. thoroughly edited the paper.

#### **Competing interests**

The authors declare no competing interests.

#### **Additional information**

**Extended data** is available for this paper at https://doi.org/10.1038/s41477-024-01788-8.

**Supplementary information** The online version contains supplementary material available at https://doi.org/10.1038/s41477-024-01788-8.

**Correspondence and requests for materials** should be addressed to Songxiao Zhong or Xiuren Zhang.

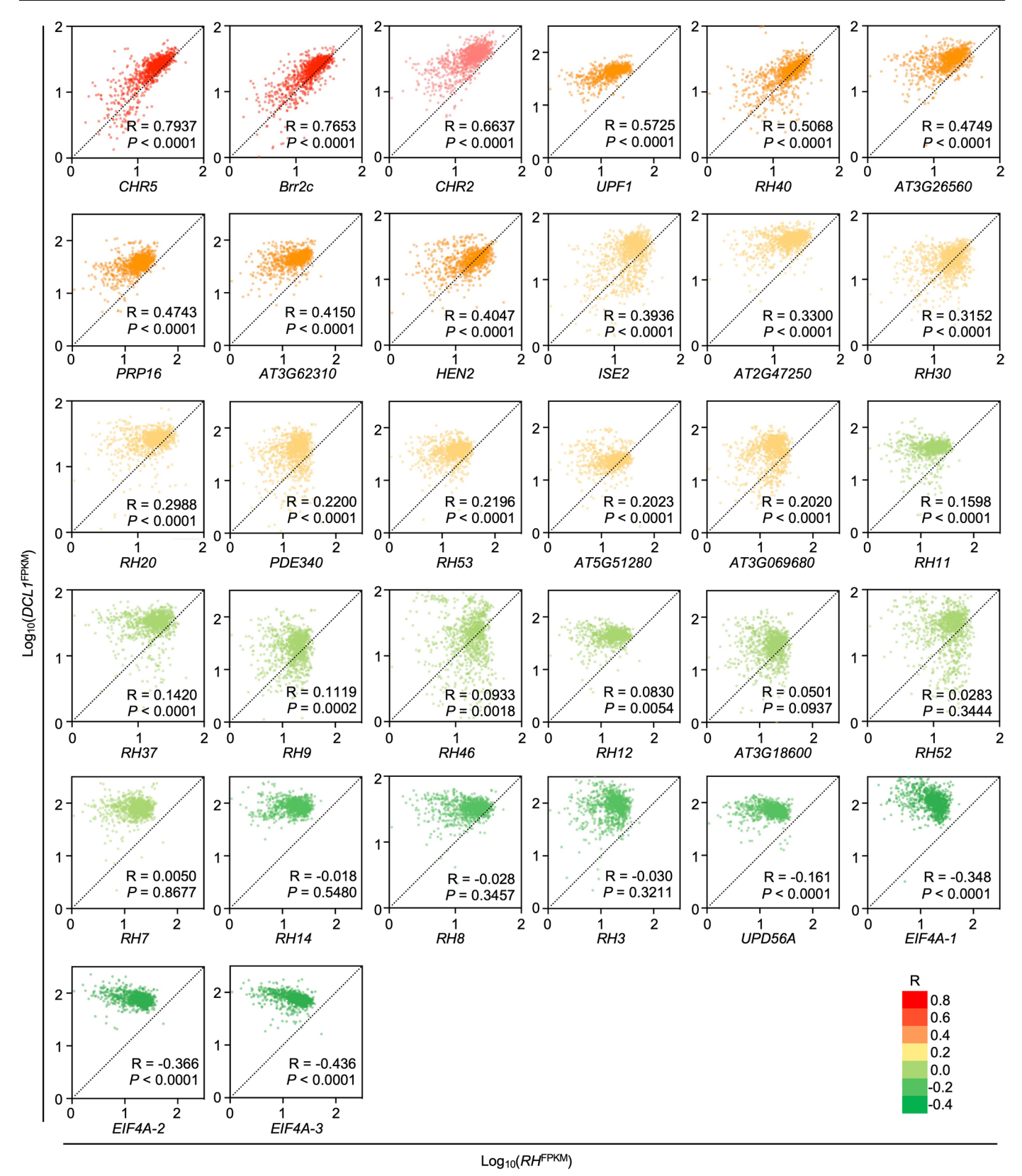
**Peer review information** *Nature Plants* thanks Lin Liu and the other, anonymous, reviewer(s) for their contribution to the peer review of this work.

**Reprints and permissions information** is available at www.nature.com/reprints.

**Publisher's note** Springer Nature remains neutral with regard to jurisdictional claims in published maps and institutional affiliations.

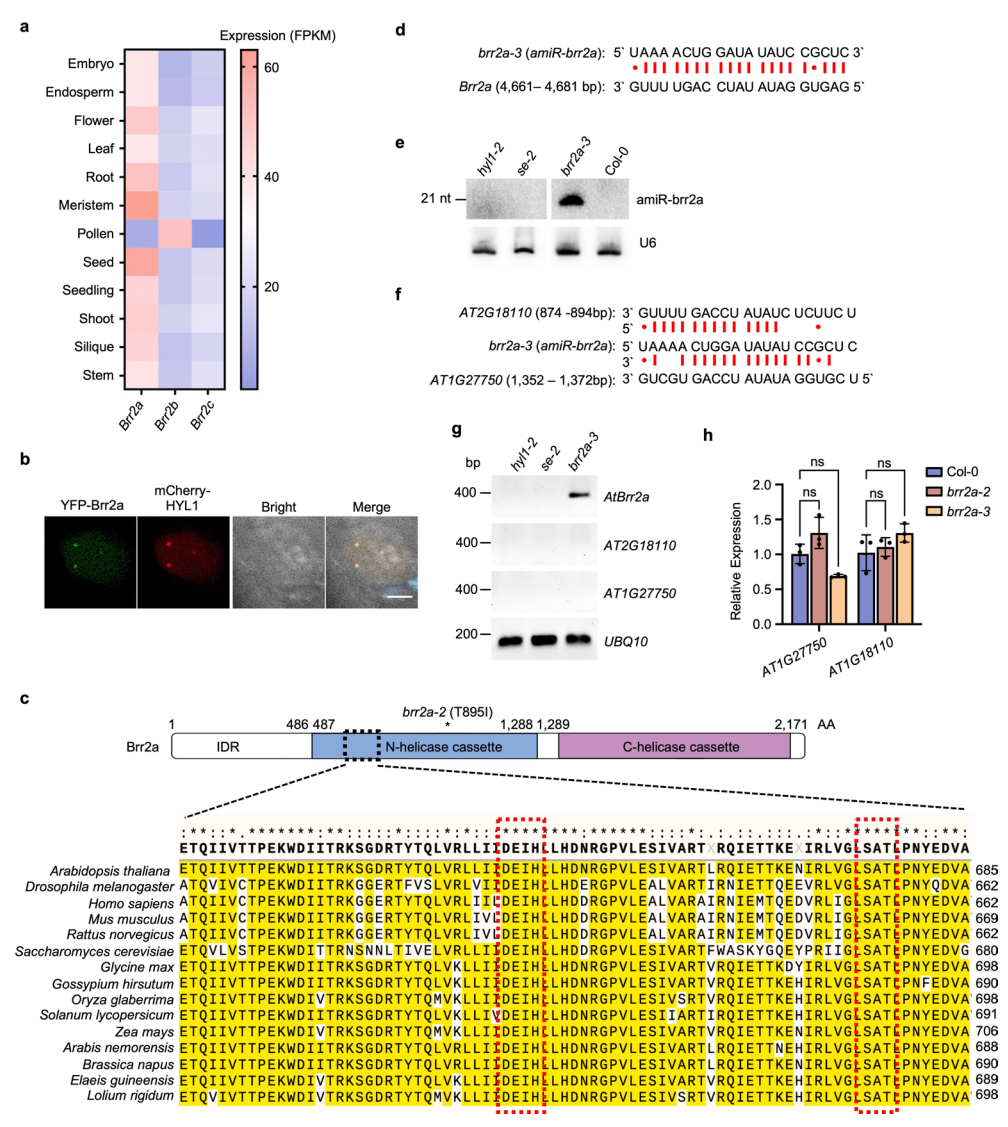
Springer Nature or its licensor (e.g. a society or other partner) holds exclusive rights to this article under a publishing agreement with the author(s) or other rightsholder(s); author self-archiving of the accepted manuscript version of this article is solely governed by the terms of such publishing agreement and applicable law.

© The Author(s), under exclusive licence to Springer Nature Limited 2024



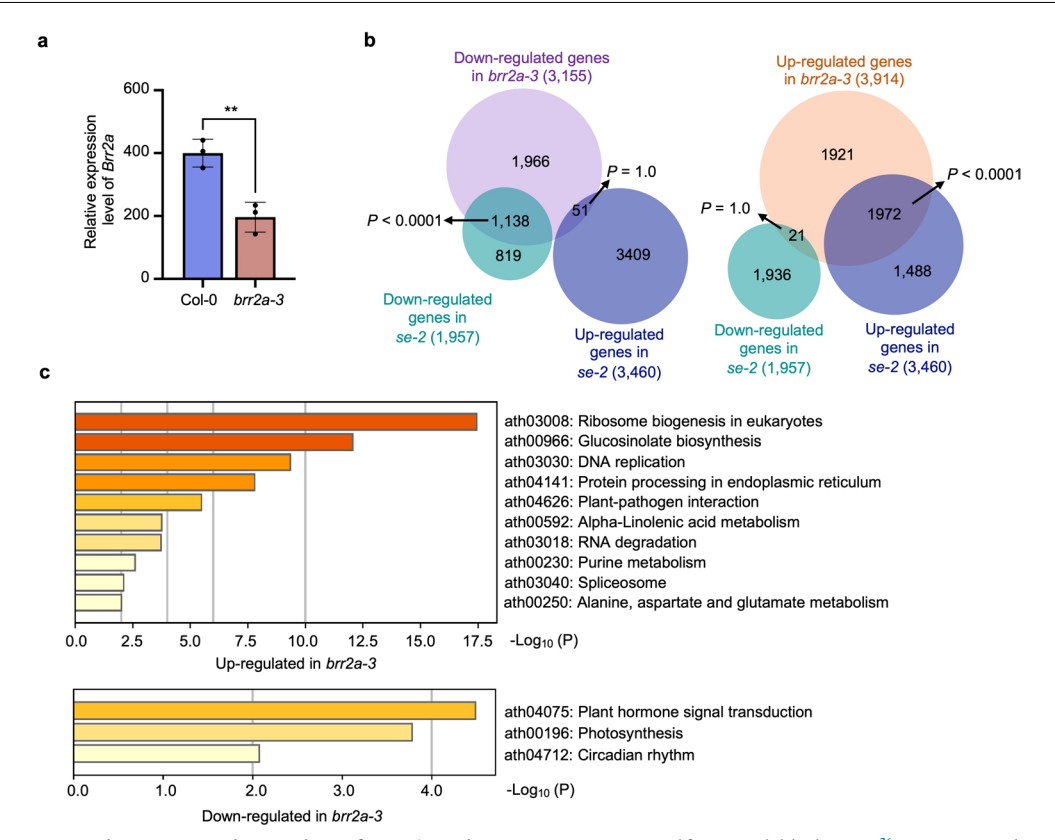
Extended Data Fig. 1 | Pan-transcriptome analysis shows different expression correlation of DCL1 and RHs. Pan-transcriptome analysis showed the expression association of DCL1 and RHs identified in IP-MS/MS of microprocessor

components. R values, Spearman's rank correlation coefficient. P values, unpaired two-sided t-test. Ns, not significant,  $P \ge 0.05$ ; \*P < 0.05; \*P < 0.05; \*\*P < 0.01; \*\*\*P < 0.001; \*\*\*P < 0.001.



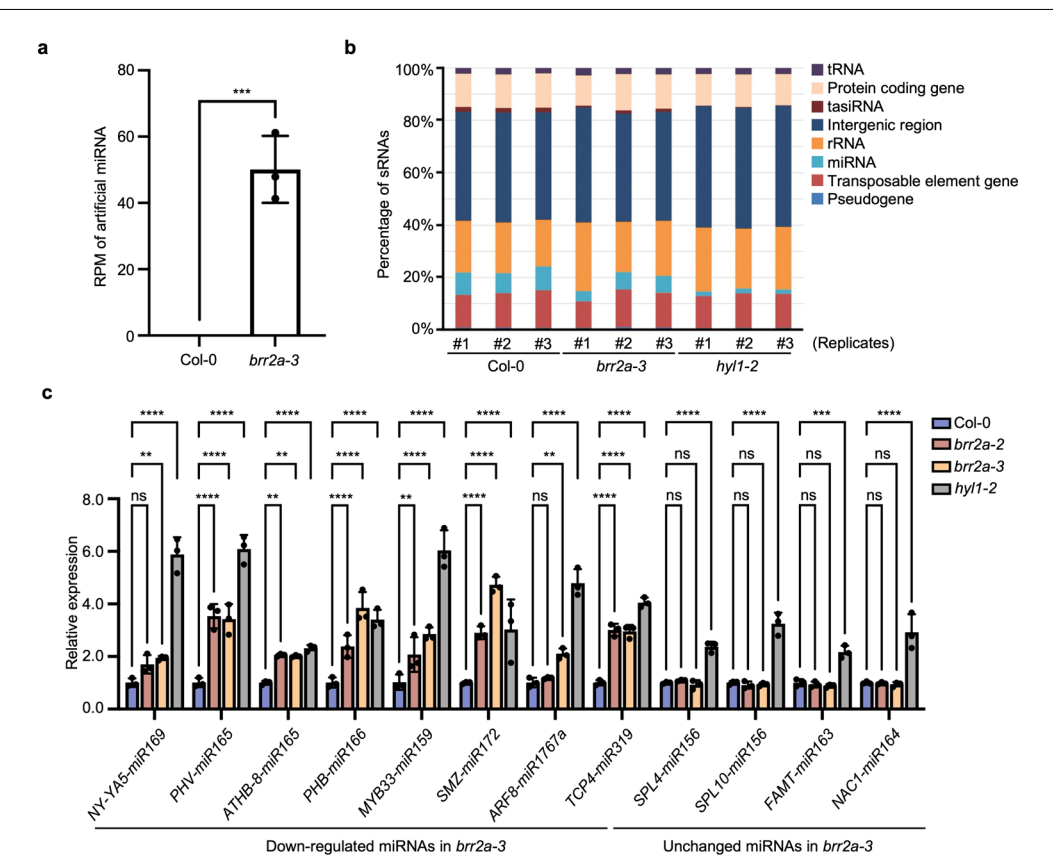
**Extended Data Fig. 2** | **Identification of** *brr2a-3.* **a**, Heatmap revealed the distinct expression levels of three Brr2 homolog genes in *Arabidopsis*. **b**, Fluorescence signal of YFP-Brr2a and mCherry-HYL1 in tobacco leaf cells. Scale bar, 5 µm. **c**, Schematic illustration of Brr2a. Multiple sequence alignment (MSA) exhibited the highly conserved the motifs associated with ATPase activity, DEIH, and RH function, SAT, within N terminal helicase cassette of Brr2a across mammals, plants, and fungi. Two motifs were highlighted by red boxes. Asterisk represented the point mutation of *brr2a-2.* **d**, Sequence alignment of the amiR-Brr2a with the transcripts of *Brr2a.* **e**, sRNA blot analyses of the artificial

miRNA in transgenic plants. Col-0 served as negative controls. U6 serves as a loading control. **f**, The sequence alignment of the amiR-Brr2a with the transcripts of putative off-targets. **g**, **h**, 5' RACE assays (**g**) and RT-qPCR (**h**) revealed the absence of off-target effects in the brr2a-3. Col-0 and brr2a-2 served as negative controls. UBQ10 was used as a loading control. Data were  $\pm$  s.d. of three biological replicates. P values, two-way ANOVA analysis with Dunnett's multiple comparisons test. Ns, not significant,  $P \ge 0.05$ . At least three independent experiments were performed, and representative images are shown (**b**, **e**, and **g**).



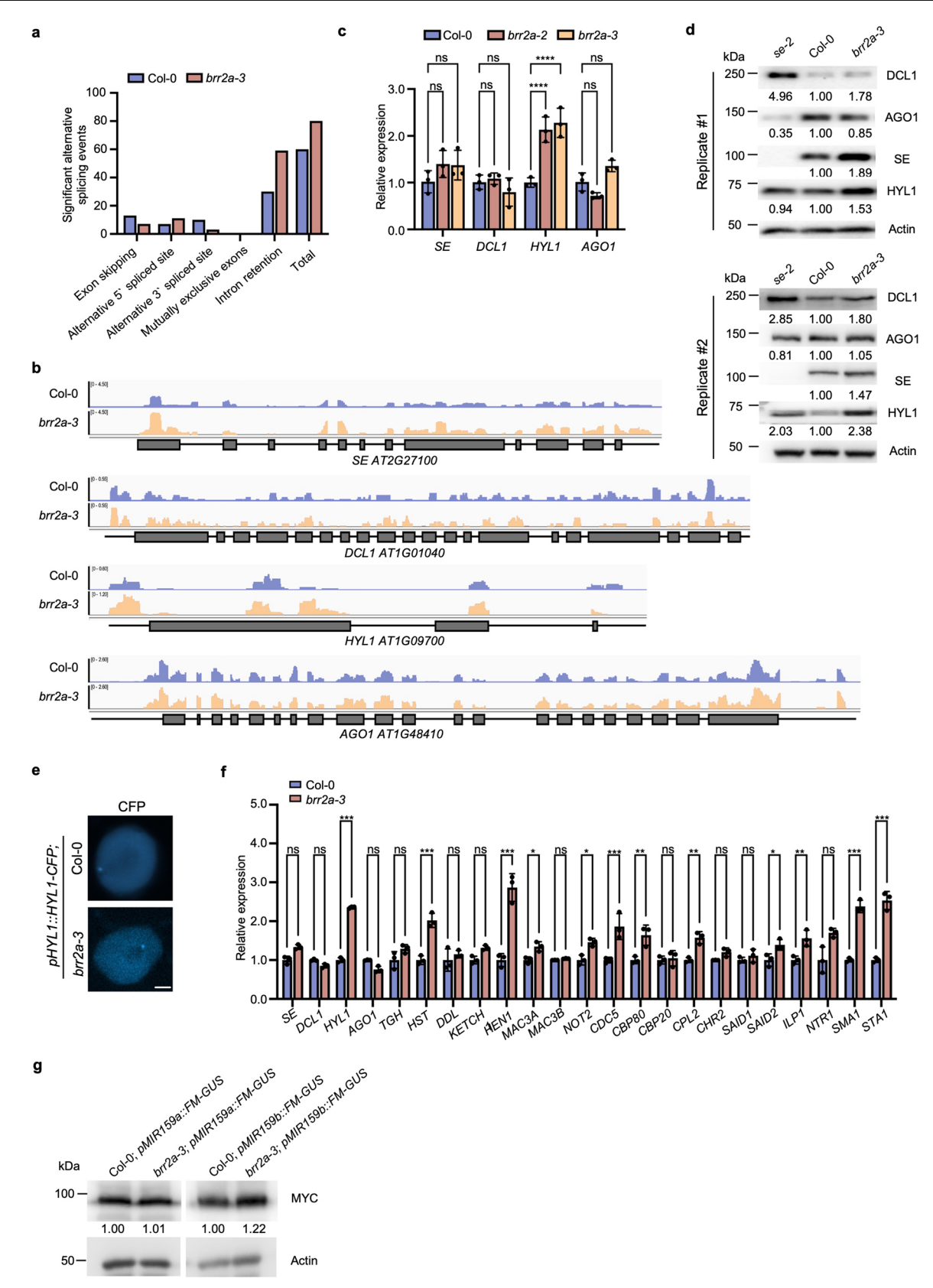
**Extended Data Fig. 3** | **Brr2a and HYL1 co-regulate a subset of genetic pathway in RNA metabolism. a**, RNA-seq analysis showed the decreased expression of Brr2a in brr2a-3 vs Col-0. Data were  $\pm$  s.d. of three biological replicates. \*\*P < 0.01. b, DEGs between brr2a-3 and se-2 were significant overlapped. RNA-seq data for

se-2 was sourced from available datasets  $^{26}$ . **c**, KEGG enrichment of DEGs in brr2a-3. P values, unpaired two-sided t-test (**a**) and hypergeometric distribution test (**b**, **c**).



**Extended Data Fig. 4** | miRNA production was compromised in *brr2a-3*. **a**, sRNA-seq analysis exhibited the significantly expression of amiR-Brr2a in *brr2a-3* vs Col-0. **b**, sRNA-seq analysis presented the sRNA species and their genomic distributions across Col-0, *brr2a-3*, and *hyl1-2*. Each sample consists of three independent biological replicates, with distinct sRNA species annotated

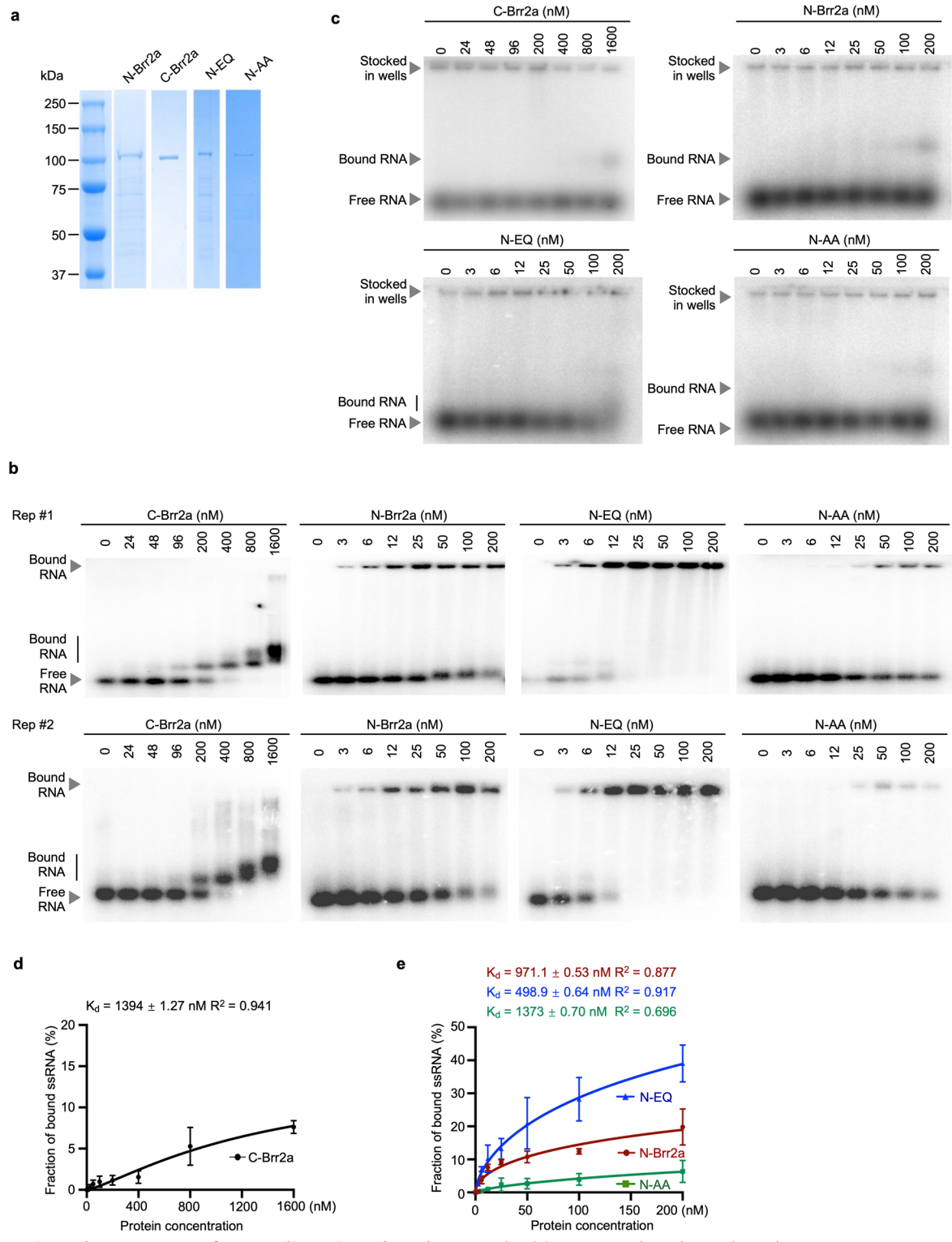
using different colors.  $\mathbf{c}$ , RT-qPCR validated that the expression of most miRNA targets was increased in brr2a-3 and hylI-2 vs Col-0. Data were  $\pm$  s.d. of three biological replicates ( $\mathbf{a}$ ,  $\mathbf{c}$ ). P values, unpaired two-tailed t-test ( $\mathbf{a}$ ) and two-way ANOVA analysis with Dunnett's multiple comparisons test ( $\mathbf{c}$ ). Ns, not significant,  $P \ge 0.05$ ; \*\*P < 0.01; \*\*\*P < 0.001; \*\*\*P < 0.0001 ( $\mathbf{a}$ ,  $\mathbf{c}$ ).



 $Extended\,Data\,Fig.\,5\,|\,See\,next\,page\,for\,caption.$ 

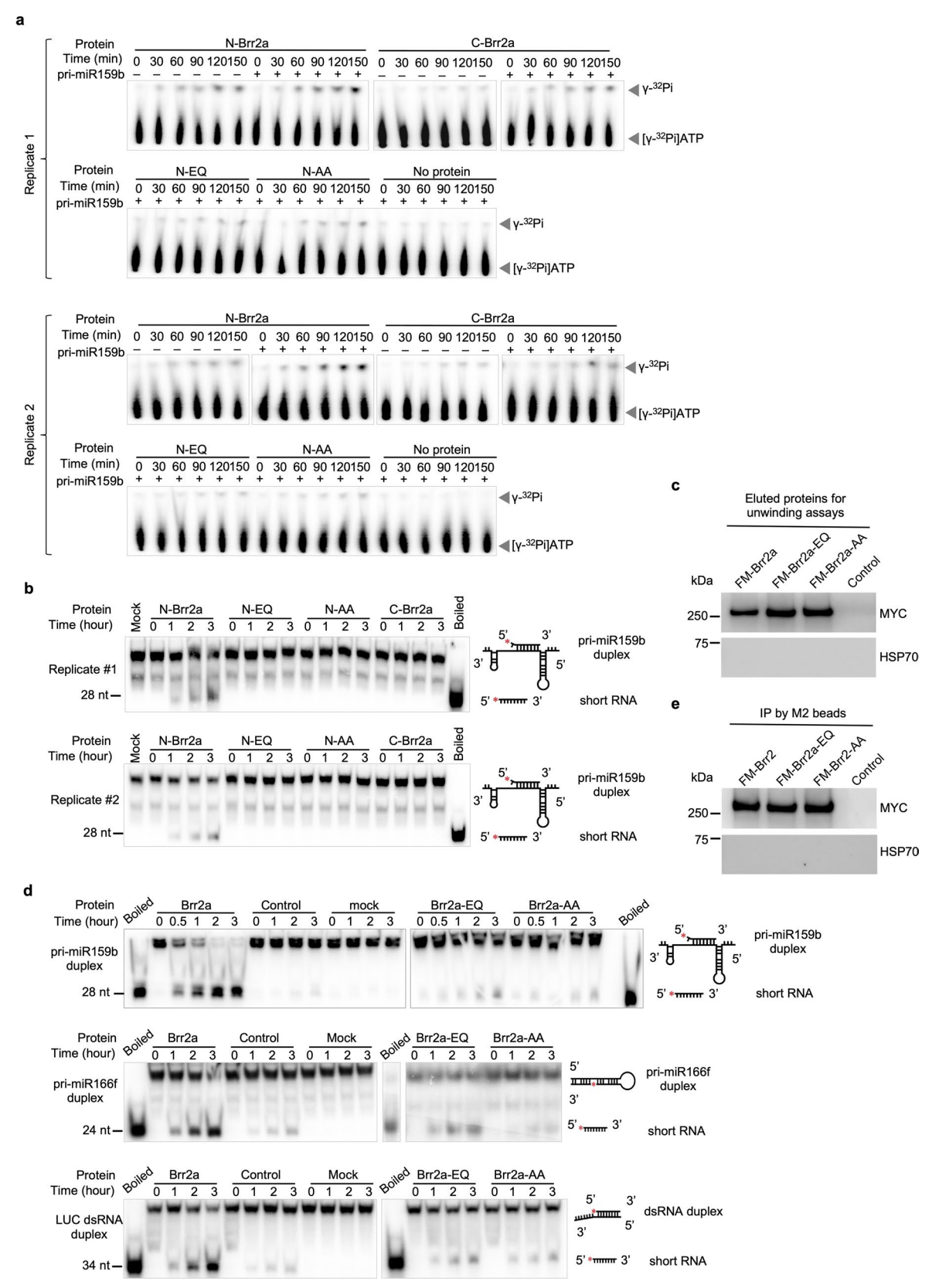
**Extended Data Fig. 5** | **Splicing of selected components in miRNA pathway remains unaffected in** *brr2a-3.* **a,** rMATs analysis exhibited the defected AS events in *brr2a-3.* **b,** IGV illustrated the integrity of selected miRNA pathway components in RNA-seq data of *brr2a-3* vs Col-0. **c,** RT-qPCR exhibited no reduction in the expression of miRNA pathway components in *brr2a* mutants vs Col-0. **d,** Western blot analysis demonstrated no reduction in the protein levels of miRNA pathway components in *brr2a-3* vs Col-0. Proteins were detected by their endogenous antibodies. Actin served as a loading control. **e,** Confocal imaging showed that Dicing body signal of HYL1 was not affected in *brr2a-3* vs Col-0. *pHYL1::HYL1-CFP* was crossed into *brr2a-3* and F2 plants was

used for microscope analysis. Scale bar, 1  $\mu$ m. **f**, RNA-seq analysis exhibited no reduction in the expression of miRNA pathway components in  $brr2a\cdot3$  mutant vs Col-0. **g**, Western blot of GUS performed with F3 segregation lines showed the comparable transcription of MIR159a/MIR159b in  $brr2a\cdot3$  vs Col-0. Total protein was extracted from a pool of at least 10 different F3 segregation lines. See also Fig. 2f for histochemical staining analysis. Data were  $\pm$  s.d. of three biological replicates (**c**, **f**). At least three biological replicates (**d**, **e**, and **g**) were performed, and representative images are shown. P values, two-way ANOVA analysis with Dunnett's multiple comparisons test (**c**) and unpaired two-tailed t-test (**f**). Ns, not significant,  $P \ge 0.05$ ; \*P < 0.05; \*P < 0.05; \*P < 0.01; \*\*\*P < 0.001; \*\*\*P < 0.001; \*\*\*\*P < 0.001; \*\*\*P < 0.001



Extended Data Fig. 6 | The two cassettes of Brr2a and its variants showed different binding ability to RNA in vitro. a, Coomassie Brilliant Blue staining of SDS-PAGE gels displayed the recombinant truncated Brr2a and its variants purified from E. coli. The experimental conditions were optimized for at least 6 times for purifying N-Brr2a and its variants and 3 times for purifying C-Brr2a and the proteins were later purified and obtained for multiple times under the best optimized conditions; and the results were always consistent.  $\mathbf{b}$ ,  $\mathbf{c}$  Two independent EMSA assays showed the distinct binding affinities of truncated Brr2a and its variants to dsRNA ( $\mathbf{b}$ ), folded pri-miR159b, and to ssRNA ( $\mathbf{c}$ ),

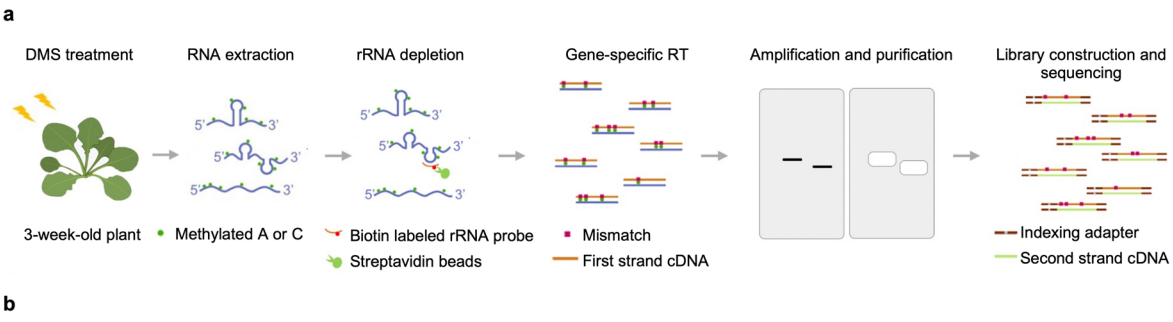
oligo(A) $_{43}$ , in vitro. At least three independent experiments were performed, and representative images are shown. **d,e**, The statistical analysis of EMSA results exhibited the distinct affinities of C-Brr2a (**d**) and N-Brr2a (**e**) and its variants to ssRNA in vitro. Data are mean  $\pm$  s.d. of three independent replicates. The  $K_d$  and  $R^2$  values were quantified from autography signal of labelled RNAs with s.d. from three independent replicates fitting a Hill slope model. For (**a-e**), N/C-Brr2a represented N/C terminal truncated Brr2a; N-EQ or N-AA represented the variants of N-Brr2a carrying mutations E640Q or S676A and T678A.

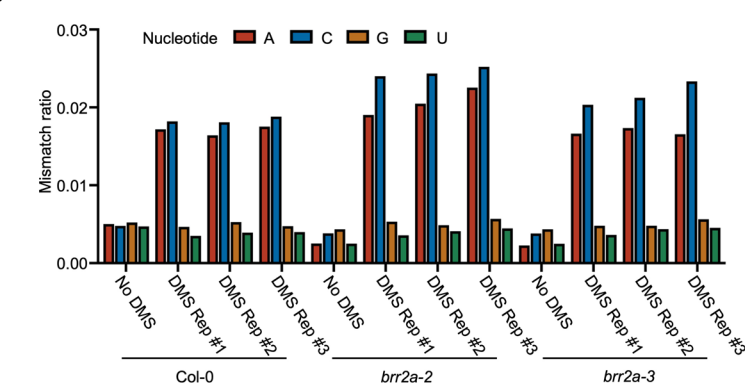


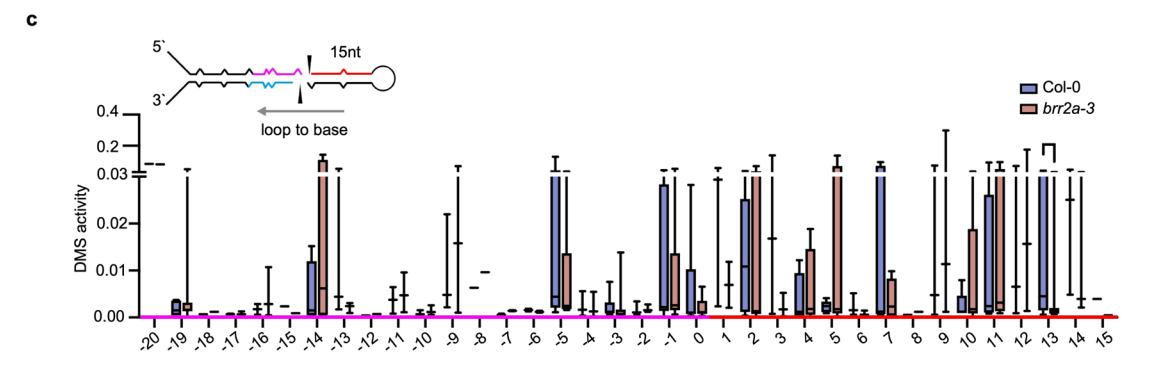
Extended Data Fig. 7 | See next page for caption.

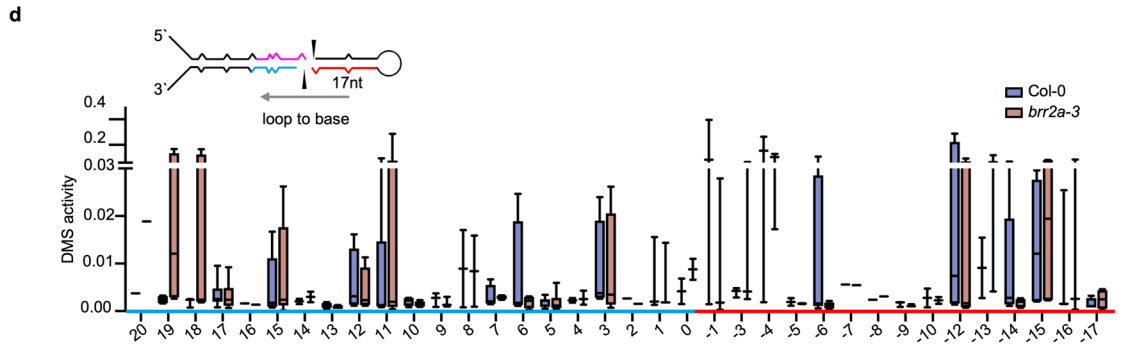
**Extended Data Fig. 7** | **Brr2a can exert its role as an RH using pri-miRNA as a substrate. a**, Two independent replicates of TLC assays showed the distinct ATPase activity of truncated Brr2a and its variants *in vitro.* **b**, Two independent replicates of unwinding assays showed the helicase activity of truncated Brr2a and its variants *in vitro.* **c**, Western blot analysis validated the comparable IP product of Brr2a and its variants used for unwinding assay. The IPs were performed using M2 beads with *brr2a-2* complementary lines, with *brr2a-2* serving as a control. Function compromised variants were slightly more concentrated during elution. Eluted proteins were detected by an anti-MYC antibody, with HSP70 serving as a control. **d**, The Native-PAGE results from an additional independent replicate of unwinding assays showed the distinct

RH activity of truncated Brr2a and its variants invitro. **e**, Western blot analysis validated the successful immunoprecipitation of Brr2a and its variants from indicated brr2a-2 complementary lines in RIP assays. The IPs were performed using M2 beads with brr2a-2 complementary lines, with brr2a-2 serving as a control. Proteins were detected by an anti-MYC antibody, with HSP70 serving as a control. At least three independent experiments were performed, and representative images are shown ( $\mathbf{a}$ - $\mathbf{d}$ ). For  $\mathbf{a}$ - $\mathbf{e}$ , N/C-Brr2a represented N/C terminal truncated Brr2a; N-EQ or N-AA represented the variants of N-Brr2a carrying mutations E640Q or S676A and T678A; Brr2a-EQ and Brr2a-AA represent the variants of full-length Brr2a carrying mutations E640Q and S676A T678A, respectively.



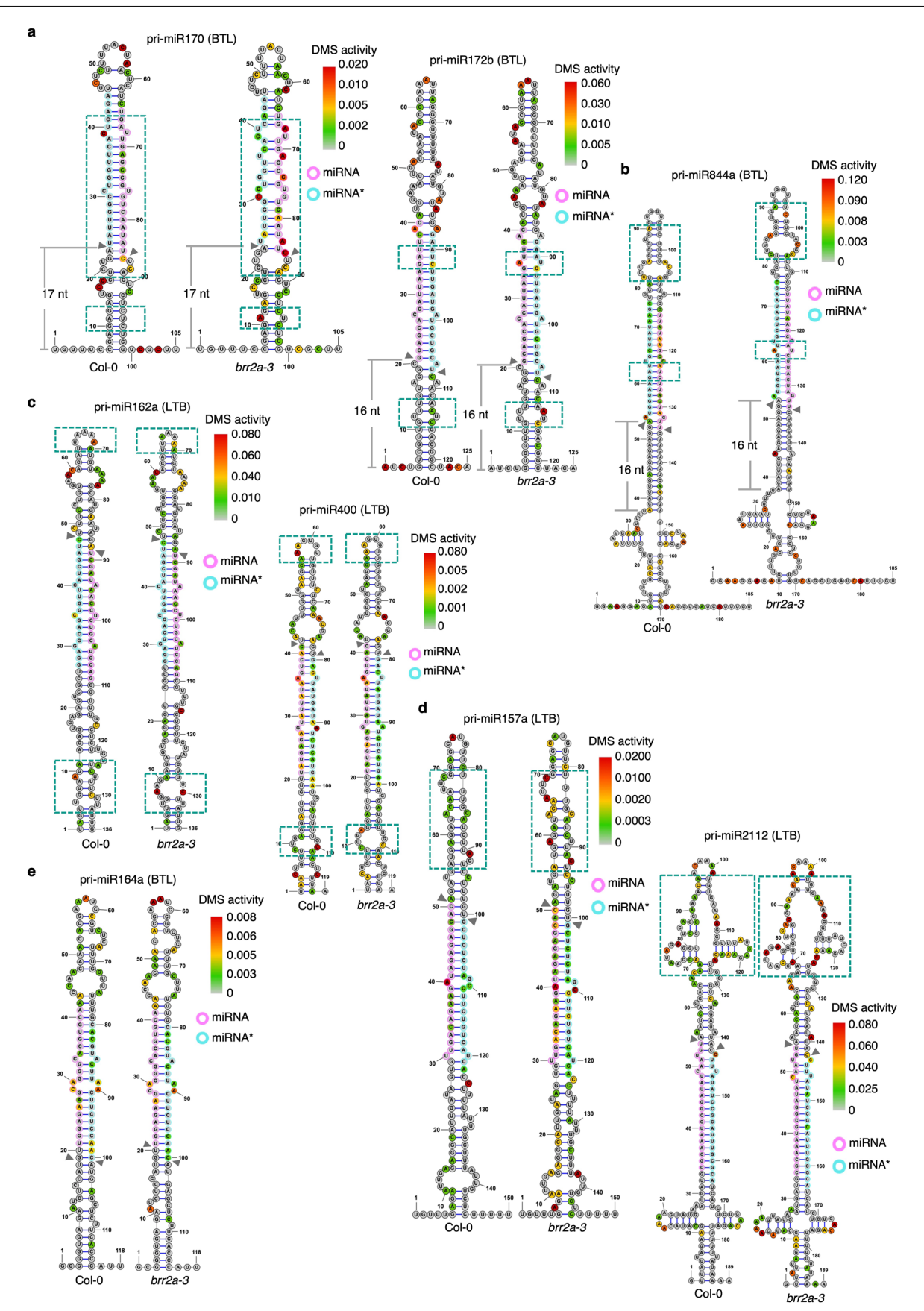






Extended Data Fig. 8 | DMS-MaPseq probes structural switch of pri-miRNAs in *brr2a-3* vs Col-0. a, Schematic approach using optimized DMS-MaPseq method to probe RSS profile of pri-miRNAs in *Arabidopsis*. b, Genome wide profile of DMS activity in *brr2a-3* vs Col-0. Averaged raw DMS reactivities (with read coverage ≥1000) at each type of nucleotides (A, C, G, and U) was calculated. Noting that a higher DMS reactivity value indicated less RNA structural complexity. Rep, replicate. c,d, Meta profile showed the structural switch at 5' arm (c) and 3' arm (d) of LTB processed pri-miRNAs in *brr2a-3* vs Col-0. The DMS activity at each site

was represented with a box plot, with the lines, box edges, and whiskers indicated the median, quartiles, and min to max respectively. In the RNA plot, as well as on the X-axis of the statistical analysis graph, upper stem and miRNA/\* duplex regions were consistently marked in red and pink/blue. Furthermore, position 0 represents the base at the processing site in the miRNA/\* region. The numerical values indicated the distance of other bases located in the miRNA/\* region or lower stem region, with negative and positive values, away from the 0th base.



Extended Data Fig. 9 | See next page for caption.

**Extended Data Fig. 9** | **Brr2a** is necessary for the proper structure of **pri-miRNAs** for processing. **a**, RSS of pri-miR170 (left) and pri-miR172b (right) exhibited structural switch at the lower stem and miRNA duplex regions, highlighted by green dashed boxes, in *brr2a-3* vs Col-0. Both pri-miR170 and pri-miR172b represented two of cases processed with BTL direction. **b**, RSS of pri-miR844a exhibited structural switch at the upper stem and miRNA/\* duplex regions in *brr2a-3* vs Col-0, with distinctions highlighted by green dashed boxes. Pri-miR844a represented one of cases processed with BTL direction. **c**, RSS of pri-miR162a and pri-miR400 exhibited structural switch at terminal loop and

lower stem in *brr2a-3* vs Col-0, with distinctions highlighted by green dashed boxes. Pri-miR162a and pri-miR400 represented cases processed by LTB direction. **d**, RSS of pri-miR157a and pri-miR2112 exhibited structural switch at upper stem in *brr2a-3* vs Col-0, with distinctions highlighted by green dashed boxes. Both pri-miR157a and pri-miR2112 displayed the structure suitable for processing in *brr2a-3* vs Col-0. Pri-miR157a and miR2112 represented two of cases processed with LTB direction. **e**, RSS of pri-miR164a exhibited similar structure in *brr2a-3* vs Col-0. For (**a**-**e**), pink and blue circles respectively represent miRNA and miRNA\*, respectively. Gray triangles label the first cutting sites.

# nature portfolio

Corresponding author(s):	Songxiao Zhong, Xiuren Zhang
Last updated by author(s):	08/09/2024

### **Reporting Summary**

Nature Portfolio wishes to improve the reproducibility of the work that we publish. This form provides structure for consistency and transparency in reporting. For further information on Nature Portfolio policies, see our <u>Editorial Policies</u> and the <u>Editorial Policy Checklist</u>.

< ∙	トつ	1		Ηı	$\sim$
. )	ıa	ш	15	u	CS

For	all statistical analyses, confirm that the following items are present in the figure legend, table legend, main text, or Methods section.
n/a	Confirmed
	The exact sample size $(n)$ for each experimental group/condition, given as a discrete number and unit of measurement
	A statement on whether measurements were taken from distinct samples or whether the same sample was measured repeatedly
	The statistical test(s) used AND whether they are one- or two-sided Only common tests should be described solely by name; describe more complex techniques in the Methods section.
X	A description of all covariates tested
	A description of any assumptions or corrections, such as tests of normality and adjustment for multiple comparisons
	A full description of the statistical parameters including central tendency (e.g. means) or other basic estimates (e.g. regression coefficient AND variation (e.g. standard deviation) or associated estimates of uncertainty (e.g. confidence intervals)
	For null hypothesis testing, the test statistic (e.g. <i>F</i> , <i>t</i> , <i>r</i> ) with confidence intervals, effect sizes, degrees of freedom and <i>P</i> value noted <i>Give P values as exact values whenever suitable.</i>
$\boxtimes$	For Bayesian analysis, information on the choice of priors and Markov chain Monte Carlo settings
X	For hierarchical and complex designs, identification of the appropriate level for tests and full reporting of outcomes
$\times$	Estimates of effect sizes (e.g. Cohen's <i>d</i> , Pearson's <i>r</i> ), indicating how they were calculated
	Our web collection on statistics for biologists contains articles on many of the points above.

#### Software and code

Policy information about availability of computer code

Data collection

For confocal microscopy assays, signals were detected with Leica stellaris 5 laser-scanning confocal microscope with LAS X Life Science Microscope Software (version 4.6.0.27096). YFP fluorescence signals were excited at 514 nm. The emissions for YFP and chlorophyll fluorescence are 525 - 550 nm, and 661 - 700 nm, respectively.

For Western blot assays, the signals were detected with ChemiDoc XRS imaging system (bioRad, version 6.1).

Small RNA sequencing and RNA sequencing data were collected using illumina HiSeq 2500 sequencing platforms.

DNAS MaRraquencing data were collected using illumina New Seq. 6000 sequencing platforms.

DMS-MaPsequencing data were cellected using illumina NovaSeq 6000 sequencing platforms.

Data analysis

For confocal microscopy assays, dat5a were analyzed with LAS X Life Science Microscope Software (version 4.6.0.27096). For the images of processing assay, western blots, and EMSA assays were quantified with imageJ (version 1.53k), the Kd and apparant Kd were calculated using Prism 9 (GraphPad, version 9.5.1).

For small RNA sequencing analysis, adaptors of sRNA reads were trimmed by cutadapt (version 3.4); reads with length between 19- to 28-nt were selected and mapped to the genome using Bowtie (version 1.2.3); bam files were sorted by SAMtools (version 1.11). Reads were counted by Subread (version 2.0.2).

For RNA sequencing, the raw data was trimmed by Cutadapt (version 1.18) and aligned by HISAT2 (version 2.1.0). The unique mapped reads were selected by SAMtools (version 1.9). Reads were counted by Subread (version 2.0.2). Integrative Genomics Viewer (version 2.12.3) was used to visualize the sequencing data.

For DMS-MaPsequencing, the raw data was trimmed by(version 1.18), filter by Fastx-toolkit (version 0.0.14), and aligned by tophat2 (version 2.1.2). Only reads that mapped uniquely selected by SAMtools (version 1.9) were retained for the identification of mismatches. Mismatch count was calculated and plotted on a bar plot using the R package "ggpubr". A Python script called CountMismatch2Bed.py (https://github.com/ changhaoli/TAMU\_02RSS) was used to call mismatches as used in https://doi.org/10.1038/s41477-024-01725-9.

For pan-transcriptome analysis, data were downloaded from http://ipf.sustech.edu.cn/pub/athrna/ and correlation analysis was calculated using Prism 9 (GraphPad, version 9.5.1).

For manuscripts utilizing custom algorithms or software that are central to the research but not yet described in published literature, software must be made available to editors and reviewers. We strongly encourage code deposition in a community repository (e.g. GitHub). See the Nature Portfolio guidelines for submitting code & software for further information.

#### Data

Policy information about availability of data

All manuscripts must include a data availability statement. This statement should provide the following information, where applicable:

- Accession codes, unique identifiers, or web links for publicly available datasets
- A description of any restrictions on data availability
- For clinical datasets or third party data, please ensure that the statement adheres to our policy

For pan-transcriptome analysis, data were downloaded from http://ipf.sustech.edu.cn/pub/athrna/

The Col-0 control for RNA-seq and sRNA-seq and the Col-0 control for DMS-MaPseq were adopted from the PRJNA613247 (https://doi.org/10.1038/s41477-020-0721-4) and PRJNA1092576 (https://doi.org/10.1038/s41477-024-01725-9) studies, respectively, since the sequence libraries of brr2a mutants were prepared simultaneously. The high-throughput sequence data can be accessed via the following link: https://www.ncbi.nlm.nih.gov/bioproject/1117818. For the convenience of readers, we have also uploaded the original data for the control groups. RNA-seq (https://doi.org/10.1093/pcp/pcp109) and sRNA-seq (https://doi.org/10.1016/j.devcel.2018.05.023) data of hyl1-2 can be access under accession numbers PRJNA116651 in the OmicsDI databases (https://www.omicsdi.org/dataset/omics\_ena\_project/PRJNA116651) and GSE111814 in the NCBI GEO database (https://www.ncbi.nlm.nih.gov/geo/query/acc.cgi?acc=GSE111814), respectively. RNA-seq data of se-2 (https://doi.org/10.1038/s41477-020-0721-4) can be accessed under accession number PRJNA613247 in the NCBI BioProject database (https://www.ncbi.nlm.nih.gov/bioproject/613247).

#### Research involving human participants, their data, or biological material

Policy information about studies with <u>human participants or human data</u>. See also policy information about <u>sex, gender (identity/presentation)</u>, and <u>sexual orientation</u> and <u>race, ethnicity and racism</u>.

Reporting on sex and gender	N/A
Reporting on race, ethnicity, or other socially relevant groupings	N/A
Population characteristics	N/A
Recruitment	N/A
Ethics oversight	N/A

Note that full information on the approval of the study protocol must also be provided in the manuscript.

### Field-specific reporting

Please select the one below	v that is the best fit for your research.	If you are not sure, read the appropriate sections before making your selection.
Life sciences	Behavioural & social sciences	Ecological, evolutionary & environmental sciences

For a reference copy of the document with all sections, see  $\underline{\text{nature.com/documents/nr-reporting-summary-flat.pdf}}$ 

### Life sciences study design

All studies must disclose on these points even when the disclosure is negative.

Sample size	No statistical method was used to pre-determine sample size. Standard sample size was chosen similar to those in PMID: 29769717 and PMID: 33288888.
Data exclusions	No data was excluded.
Replication	All experiments were independently repeated more than three times with similar results obtained, and the exact replicate numbers are provided in the respective figure legends.
Randomization	Plants were randomly assigned to experimental groups whenever possible. For other experiments, the experiments were randomized and the investigators were blinded to allocation.
Blinding	The experiments were randomized and the investigators were blinded to allocation.

### Reporting for specific materials, systems and methods

We require information from authors about some types of materials, experimental systems and methods used in many studies. Here, indicate whether each material, system or method listed is relevant to your study. If you are not sure if a list item applies to your research, read the appropriate section before selecting a response.

Materials & experime	ental systems Methods
n/a Involved in the study	n/a Involved in the study
Antibodies	ChIP-seq
Eukaryotic cell lines	Flow cytometry
Palaeontology and a	archaeology MRI-based neuroimaging
Animals and other o	organisms .
Clinical data	
Dual use research o	of concern
☐ X Plants	
1	
Antibodies	
	AA - I - I - 1: FLAC (C: ALL: I - A0F02 I A42 ID 1 F000)
Antibodies used	Monoclonal anti-FLAG (Sigma-Aldrich, A8592,clone: M2, IB 1:5000) Monoclonal mouse anti-MYC (Sigma-Aldrich, C3956, 9E10, IB 1:5000)
	Polyclonal rabbit NRPB2 (PyhtoAB, PHY2429S, IChIP 1:250, IB: 1:1000)
	Mouse monoclonal anti-actin (Sigma-Aldrich, A0480, clone:10-B3, IB 1:5000),
	Polyclonal rabbit anti-AGO1 (Agrisera, ASO9 527, IB 1:1000) Polyclonal rabbit anti-SE (Seong Wook Yang's Lab, 1:5000 dilution, PMID: 32690892)
	Polyclonal rabbit anti-HYL1 (Seong Wook Yang's Lab, PMID: 32690892)
	Polyclonal rabbit anti-DCL1 (Agrisera, AS12 2102, IB 1:1000)
	Polyclonal rabbit anti-HSP70 (Agrisera, AS08 371, IB 1:5000)
	IgG from huamn serum (Sigma-Aldrich, I4506, 3 µg per reaction) Secondary antibodies were goat-developed anti-rabbit (Cytiva, NA934NA934, IB 1:3000) and anti-mouse IgG (Cytiva, NA931, IB
	1:3000)
	Secondary antibodies used in this study were anti-rabbit (GE Healthcare, NA934) and anti-mouse IgG (GE Healthcare, NA931).
Validation	Monoclonal anti-FLAG, https://www.sigmaaldrich.com/US/en/product/sigma/a8592
vandation	Mouse monoclonal anti-actin, https://www.sigmaaldrich.com/US/en/product/sigma/a0480, and see also validation in PMID:
	32690892
	Monoclonal mouse anti-MYC, https://www.sigmaaldrich.com/US/en/product/sigma/c3956 Polyclonal rabbit NRPB2, https://www.phytoab.com/nrpb2%20antibody
	Polyclonal rabbit anti-AGO1, https://www.agrisera.com/en/artiklar/ago1-argonaute-1.html, and see also validation in PMID:
	32690892
	Polyclonal rabbit anti-SE (PMID: 32690892)
	Polyclonal rabbit anti-HYL1 (PMID: 32690892) Polyclonal rabbit anti-DCL1 (PMID: 32690892)
	Polyclonal rabbit anti-HSP70, https://www.agrisera.com/en/artiklar/hsp70-heat-shock-protein-70-cytoplasmic.html
	IgG from huamn serum, https://www.sigmaaldrich.com/US/en/product/sigma/i4506
	Anti-rabbit, https://www.sigmaaldrich.com/US/en/product/sigma/gena9341ml, and see also validation in PMID: 32690892
	Anti-mouse, https://www.sigmaaldrich.com/US/en/product/sigma/gena9311ml, and see also validation in PMID: 32690892
	All commercial antibodies used were validated by original companies and inhouse with Arabidopsis proteins. All homemade antibodies used were validated by inhouse with Arabidopsis proteins and recombinant proteins.

### Dual use research of concern

Policy information about <u>dual use research of concern</u>

#### Hazards

Could the accidental, deliberate or reckless misuse of agents or technologies generated in the work, or the application of information presented in the manuscript, pose a threat to:

No Yes		
Public health		
National security		
Crops and/or lives	stock	
Ecosystems		
Any other signification	ant area	
Experiments of conce	rn	
Does the work involve a	ny of these experiments of concern:	
No Yes		
Demonstrate how	to render a vaccine ineffective	
Confer resistance		
Enhance the virul	Enhance the virulence of a pathogen or render a nonpathogen virulent	
Increase transmis	Increase transmissibility of a pathogen	
Alter the host ran	ge of a pathogen	
Enable evasion of	diagnostic/detection modalities	
Enable the weapo	—   —	
Any other potentially harmful combination of experiments and agents		
Plants		
Seed stocks	Seeds of se-2 (SAIL_44_G12) and hyl1-2 (SALK_064863) were obtained from Arabidopsis Biological Resource Center. Seeds of brr2a-2 were obtained from Dr. L. Hennig. Artifical miRNA knock-down transgenic plants of amiR-brr2a were generated by xiuren zhang's lab in this study.	
Novel plant genotypes In summary, the amiR-brr2a exhibit developmental defects including irregular leaf shapes, serration, reduced plant stature development, and changed flowering time.		

Seeds of se-2 (SAIL\_44\_G12) and hyl1-2 (SALK\_064863) were authenticated by Arabidopsis Biological Resource Center. Seeds of brr2a-2 were authenticated by Dr. L. Hennig's.

Authentication